teins are implicated in cholesterol homeostasis, phospholipid metabolism, vesicular transport, and cell signaling (55). OSBP functions as sterol sensor that regulates the transport of ceramide from the ER to the Golgi apparatus for de novo synthesis of sphingomyelin by coordinated action with ceramide transport protein (CERT) (36). OSBP also functions as a scaffolding protein for two phosphatases (phosphatase 2A/HePTP) (49). This complex regulates the activity of extracellular signal-regulate kinase. This cytosolic 440-kDa complex disassembles by the addition of 25-hydroxycholesterol (25-HC) or depletion of cholesterol, both of which cause OSBP translocation to the Golgi compartment (49). Thus, in addition to its role in intracellular trafficking, OSBP appears to regulate cell signaling. We investigated the functional significance of OSBP association with HCV RNP complexes. RNA interference studies support a functional role of OSBP in virion morphogenesis and release process. The OSBP PH domain deletion mutant (ΔPH) failed to localize to the Golgi apparatus and caused an inhibition of the HCV particle release. Our work described herein also demonstrates that the association of OSBP with NS5A may also contribute to the overall HCV maturation process.

MATERIALS AND METHODS

Plasmids. The plasmids pJFH1, pSGR-JFH1, and pSGR-Luc-JFH1 were the generous gift of T. Wakita (22, 48). pSGR-JFH1-5A1ST, in which NS5A gene contains the One-STrEP tag (IBA, Göttingen, Germany), was generated by PCR-mediated mutagenesis using oligonucleotides described in Table S1 in the supplemental material. pFL-Luc-Jc1, an analogue to Luc-Jc1 (23), was constructed as described in Table S1 in the supplemental material. For constructing the human OSBP expression vector pFLAG-CMV-OSBP (where CMV is cytomegalovirus), OSBP1 cDNA was amplified from total RNA extracted from Huh7 cells by reverse transcription-PCR (RT-PCR), using oligonucleotides described in Table S1 in the supplemental material, and amplified product was digested with both HindIII and BamHI and cloned into the corresponding sites in the pFLAG-CMV2 vector (Sigma-Aldrich, St. Louis, MO). Expression vectors for mutant forms of OSBPs were constructed as described in Table S1 in the supplemental material. The VAP-A expression vector, pEF-FLAG-VAP-A, was kindly provided by Y. Matsuura (17). Generation of NS5A deletion mutants has been described previously (20). The NS5A derived from HCV JFH1 (genotype 2a) was cloned in the pEF1/Myc-His vector (Invitrogen, Carlsbad, CA) at the KpnI and XbaI sites by using a PCR-amplified fragment using primers described in Table S1 in the supplemental material. Lentiviral vectors, L-CMV-GFP-NheI (where GFP is green fluorescent protein), and packaging plasmids pMDL, pVSV-G (where VSV-G is vesicular stomatitis virus glycoprotein), and pREV were kindly provided by I. Verma (Salk Institute, La Jolla, CA) (46) and used for cloning short hairpin RNAs (shRNAs). The oligonucleotides used for constructing a scrambled shRNA (unrelated) and the OSBP-specific shRNA-1 and shRNA-2 are described in Table S1 in the supplemental material.

Cell culture. Human hepatoma cell lines Huh7 and Huh7.5.1 were maintained in Dulbecco's modified Eagle's medium supplemented with 10% fetal bovine serum, 100 U/ml penicillin, 100 μg/ml streptomycin, and 1 mM minimal essential medium with nonessential amino acids (Invitrogen, Carlsbad, CA). The Huh7.5.1 cell line was a kind gift of F. Chisari (Scripps Institute, La Jolla, CA).

In vitro RNA transcription and RNA transfection. The plasmid encoding HCV (JFH1) was linearized by XbaI digestion, followed by mung bean nuclease treatment to blunt the XbaI-digested termini, and served as a template for RNA synthesis using a RiboMAX Large Scale RNA production system-T7 (Promega, Madison, WI). Synthesized RNAs were extracted by the acid guanidium thiocyanate phenol-chloroform (AGPC) method prior to transfection (7). Electroporation was used for RNA transfection. Subconfluent Huh7 or Huh7.5.1 cells were trypsinized and washed with ice-cold phosphate-buffered saline (PBS) and resuspended at 1×10^7 cells/ml in Cytomix buffer (47). Synthesized RNAs were mixed in 0.4 ml of cell suspension in a 4-mm gap electroporation cuvette (Genesee Scientific, San Diego, CA), pulsed at 260 V for 25 ms in a square wave mode of Gene Pulser Xcell electroporation system (Bio-Rad, Hercules, CA). For developing subgenomic replicon cell lines, Huh7 cells were transfected with in vitro synthesized replicon RNAs, incubated for 48 h in complete medium, and maintained in the presence of G418 (300 μg/ml). Stably expressing subgenomic replicon colonies were isolated after 3 weeks of growth in the presence of G418.

Proteomics analysis. Subgenomic replicon cell lines were established by transfecting SGR-JFH1 or SGR-JFH1-5A1ST RNA into Huh7 cells as described above, and isolated cell lines were designated SGR-JFH1 and SGR-JFH1-5A1ST, respectively. The NS5A protein complexes were purified by affinity chromatography from whole-cell lysates of the SGR-JFH1-5A1ST clone. Briefly, semiconfluent cell monolayers on 100-mm dishes were lysed with 4 ml of lysis buffer (0.2% deoxycholic acid, 0.25 M sucrose, 0.1 mM EDTA, and 3 mM Tris-HCl, pH 7.4) and incubated on ice for 20 min. The protein lysates were centrifuged at 25,000 × *g* for 30 min at 4°C. The cleared lysates were dialyzed against binding buffer (100 mM Tris-HCl, 150 mM NaCl, and 0.1% octylglucoside) and centrifuged again at 25,000 × *g* for 30 min at 4°C. The cleared lysates were loaded onto a StrepTactin-Sepharose column (1-ml bed volume; IBA) by filtering through 0.45-μm-pore-size polyethersulfone filter (Corning) and fractionated according to the manufacturer's instructions. The peak NS5A fraction from 30 preparations (12.5 μg) was collected and concentrated by acetone-methanol precipitation and subjected to multidimensional protein identification technology (MudPIT) analysis (5, 8, 9, 11, 26, 34, 39, 41). For the details of MudPIT analysis, see Materials and Methods in the supplemental material.

HCV infection and focus-forming unit assay. HCV JFH1 strain (48) was used for the production of HCV infectious viral particles. Huh7.5.1 cells were transfected with the in vitro synthesized RNA by electroporation. Ten days posttransfection cultured supernatants were collected. The infectious virion titers of collected supernatants were determined by a focus-forming-unit assay as described previously (58). HCV infection was performed at a multiplicity of infection (MOI) of 1.

Real-time RT-PCR. Total cellular RNAs were purified by the AGPC method (7). Viral RNAs were extracted from 100 μl of supernatant by the AGPC method. Five micrograms of *Saccharomyces cerevisiae* tRNA was added as a carrier (Sigma-Aldrich). HCV RNA was quantified on an ABI Prism 7000 sequence detection system (Applied Biosystems, Foster City, CA) as described previously (43). For the quantification of OSBP mRNA, 100 ng of total cellular RNA was subjected to cDNA synthesis using Improm II reverse transcriptase (Promega) oligo(dT) as a primer. Molecular copy number of OSBP and glyceraldehyde-3-phosphate dehydrogenase (GAPDH) cDNA was quantified by real-time PCR using SYBR premix Ex *Taq* (Takara Mirus Bio, Madison, WI) in an absolute quantification manner. The following set of primers was used for quantitative PCR: OSBP sense, 5′-AGAATACCCTTCGGACCCTCTC-3′; OSBP antisense, 5′-TCTTTTCATTGCTCTCAGCAGG-3′; GAPDH sense, 5′-GCCA TCAATGACCCCTTCATT-3′; and GAPDH antisense, 5′-TTGACGGTGCCA TGGAATTT-3′.

Western blotting analysis and immunoprecipitation. Huh7 cells or HCV-infected Huh7 cells were transfected with the indicated expression vectors by lipofection using TransIT-LT1 reagent (Mirus Bio, Madison, WI). Cells grown in a 35-mm dish were transiently transfected and incubated for 24 h, washed once with ice-cold PBS, and lysed on ice with 500 μl of lysis buffer (0.2% [wt/vol] deoxycholic acid, 20 mM Tris-HCl, 150 mM NaCl, 0.1 mM EDTA, 250 mM sucrose), supplemented with 1× Halt protease inhibitor single-use cocktail (Thermo Scientific, Rockford, IL). The cellular lysates were subjected to brief sonication, followed by centrifugation at 13,400 × *g* for 10 min. The clarified lysates were incubated with 5 μg of anti-FLAG M2 monoclonal antibody (Sigma-Aldrich) for 1 h. Five microliters of protein G-Sepharose 4 Fast Flow was added (GE Healthcare, Piscataway, NJ) for 2 h. Sepharose beads were collected by centrifugation and washed four times with 1 ml of lysis buffer. The immunoprecipitates were analyzed by sodium dodecyl sulfate-polyacrylamide gel electrophoresis. Immunoblotting analysis was performed as described previously (52). The following antibodies were used for Western blotting analysis: mouse monoclonal anticore (Affinity Bioreagents, Golden, CO), goat polyclonal anti-OSBP (Novus biological, Littleton, CO), goat polyclonal anti-ApoB (Chemicon International, Temecula, CA), rabbit polyclonal anti-human albumin (MP Biomedicals, Solon, OH), rabbit polyclonal anti-adipose differentiation-related protein (Novus Biological), mouse monoclonal anti-fatty acid synthase (BD Bioscience), mouse monoclonal anti-NS3 (Virogen), and monoclonal antibody 9E10/A3 for NS5A (a generous gift from C. Rice).

Immunofluorescence microscopy. Infected and/or transfected cells were grown on glass coverslips, washed twice with PBS, and fixed in 3% paraformaldehyde in PBS supplemented with 2 mM $MgCl_2$ and 1.25 mM EGTA for 20 m at room temperature. Fixed cells were permeabilized and blocked in antibody-binding buffer (PBS, 0.2% [wt/vol] saponin, 0.2% [wt/vol] nonfat dry milk, 1% [wt/vol] bovine serum albumin, and 0.02% sodium azide) for 2 h at 4°C. Fixed cells were incubated in the presence of primary antibodies overnight. The primary antibodies used for immunofluorescence were mouse monoclonal 9E10/A3 for NS5A,

goat polyclonal anti-OSBP (Novus), rabbit polyclonal anti-TGN46 (*trans*-Golgi network protein 46 kDa; Sigma-Aldrich), and rabbit polyclonal anti-FLAG (Anaspec, San Jose, CA) to detect FLAG-tagged proteins. Coverslips were washed three times with PBS and once with antibody-binding buffer, followed by the incubation with corresponding secondary antibodies for the detection of primary antibodies. These were donkey antibodies against mouse (DyLight 488), rabbit (DyLight 549), and goat (DyLight 649; Rockland Immunochemicals, Gilbertsville, PA). The slides were analyzed by confocal laser scanning microscopy (Zeiss LSM 510), using 488-nm, 543-nm, and 633-nm laser lines. The nuclei were counterstained by DAPI (4′,6′-diamidino-2-phenylindole) (Invitrogen, Carlsbad, CA).

RESULTS

Identification of host factors associated with RNP complexes. To identify host factors involved in HCV RNA replication, we employed an affinity-based purification procedure to isolate RNP complexes under nondenaturing conditions. We inserted an affinity tag peptide called One-STrEP-tag (28 amino acid residues) in the C-terminal region of NS5A of subgenomic replicon constructs (see Fig. S1A in the supplemental material) and established stable replicon cell lines. This insertion did not interfere with the replication of HCV replicon RNA (see Fig. S1B in the supplemental material) and/or developing G418-resistant clones (see Fig. S1C in the supplemental material). We developed, a one-step, nondenaturing affinity column chromatography procedure for the isolation of NS5A-binding proteins or protein complexes. Purified protein complexes were analyzed by Western blot assay (see Fig. S2A and B in the supplemental material). Viral protein complexes purified by this method were subjected to proteomic MudPIT analysis, which revealed a large repertoire of cellular factors (see Tables S2 to S7 in the supplemental material) and included all the viral NS proteins. Western blot analysis of the isolated proteins demonstrated the association of host factors that were identified by proteomic analysis (see Fig. S2C, right panels, in the supplemental material). In this analysis, we chose proteins whose peptide spectrum counts were significantly high. Figure S2C in the supplemental material shows the association of ApoB, OSBP, adipose differentiation-related protein, and fatty acid synthase along with the representative HCV NS proteins, NS5A and NS3. In contrast, these proteins, including NS5A, were not detected in the eluted fractions prepared from wild-type replicon (without the One-STrEP-tag) lysates (see Fig. S2C, left panels, in the supplemental material). In this study, we focused on the association of OSBP and investigated its functional relevance in the cycles of HCV infection.

Downregulation of OSBP protein affects HCV replication and viral particle release. To demonstrate the functional role of this interaction, we employed RNA interference strategy. We developed lentiviral vectors encoding two OSBP-specific shRNAs (shRNA-1 and -2). These shRNAs have been previously reported to suppress OSBP mRNA synthesis effectively (31, 36). Huh7.5.1 cells were first infected with either of the lentiviral particle-encoding shRNAs and subsequently challenged with tissue culture-grown HCV particles at an MOI of 1. A lentivirus encoding a scrambled shRNA was used as a negative control. OSBP expression was monitored by Western blot assays (Fig. 1A) and by RT-PCR analysis (Fig. 1B). Cells expressing OSBP shRNA-1 and -2 displayed differential levels of suppression of OSBP protein (Fig. 1A, top). OSBP protein was barely detectable in shRNA-1-expressing cells. On the other hand, the reduction of OSBP was modest in shRNA-2-expressing cells. OSBP protein appears as a doublet representing differentially phosphorylated forms. Albumin levels were uniformly expressed in these lysates (Fig. 1A, second panel). We examined the expression of viral core and NS5A proteins, which reflected the profile of OSBP protein expression. Both viral proteins were barely detectable in shRNA-1-expressing cells, where OSBP proteins were severely depleted, indicating a functional role of OSBP in viral translation/replication. shRNA-2, on the other hand, modestly reduced their expression (Fig. 1, lower panels). We next performed quantitative RT-PCR analyses of OSBP mRNA and viral RNAs isolated from cellular extracts (intracellular) and culture supernatants (extracellular). Intracellular RNA levels indicate viral replication, whereas extracellular viral RNA is a measure of released viral particles in the culture supernatant. The results show that both shRNAs were effective in suppressing OSBP mRNA synthesis (63% and 53%, respectively, for shRNA-1 and -2) without affecting GAPDH mRNA levels (Fig. 1B and C). The unrelated scrambled shRNA (control) did not have any effect on OSBP mRNA synthesis (Fig. 1C). shRNA-1, which was more potent in silencing the OSBP mRNA (63% reduction) (Fig. 1B), significantly suppressed intracellular levels of HCV RNA (85% reduction) (Fig. 1D). shRNA-2, on the other hand, which caused a modest reduction of OSBP mRNA (53%) compared to the shRNA-1 (Fig. 1B), reduced the intracellular HCV RNA replication levels only modestly (14%) (Fig. 1D). When levels of extracellular virion RNA were analyzed, both shRNA-1 and -2 effectively blocked the release of viral particles in the culture medium (99.8% and 87.2% reduction, respectively) (Fig. 1E). More importantly, the shRNA-2, which has little effect on intracellular HCV RNA replication levels, dramatically reduced HCV release (Fig. 1E). We further confirmed these results by determining the number of focus-forming units of the cultured supernatant as described previously (58). The culture supernatant from HCV-infected cells, which was previously infected with lentiviral vector expressing scrambled (negative control) shRNA, yielded 6×10^4 focus-forming units per ml of supernatant, whereas supernatants from shRNA-1- and shRNA-2-expressing cells displayed significantly reduced infectious virion titers, indicating that OSBP depletion effectively attenuated the rate of infectious virion release (99.8% and 84.7%, respectively) (Fig. 1F). This result confirms the previous observation that shRNA-2, which does not affect HCV replication levels (intracellular levels), dramatically affected the accumulation of extracellular viral particles (Fig. 1, compare D with E and F). Taken together, these results indicate that OSBP expression is required for both viral replication and release of viral particles.

OSBP affects virus secretion. One of the unique characteristics of the OSBP protein is its ability to translocate to the Golgi apparatus upon ligand binding. The translocalization of OSBP is regulated by its PH domain, which binds to Golgi lipids such as PI4P (Fig. 2A). The RNA interference studies described above suggest that partial depletion of OSBP can cause inhibition of viral particle secretion. To elucidate the functional role of OSBP in virion maturation processes further, we generated several mutants of OSBP (Fig. 2B). These include an N-terminal region of OSBP containing only the PH domain fragment (N-PH), a deletion in the PH domain (ΔPH),

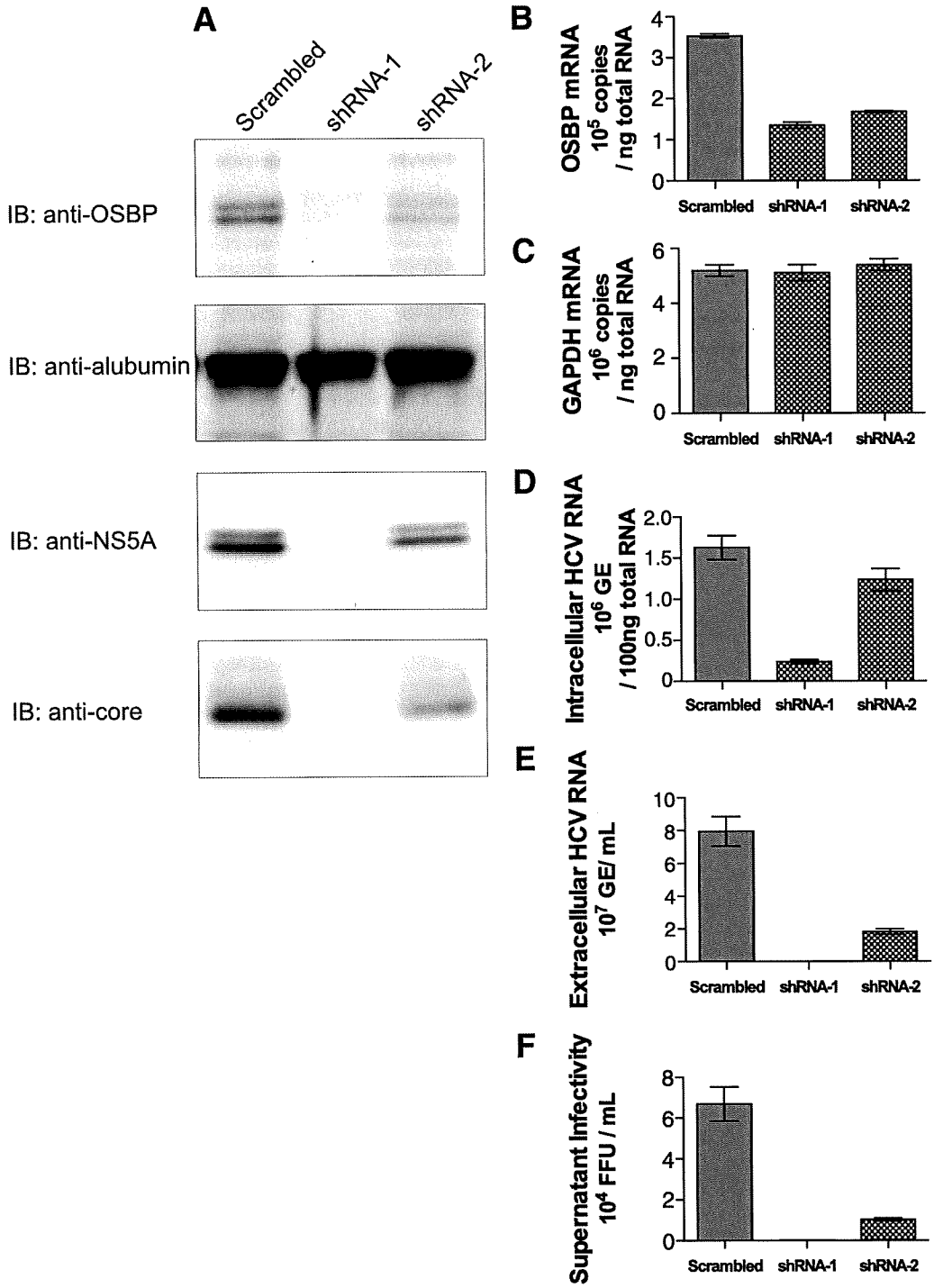

FIG. 1. Effect of silencing OSBP on HCV replication and viral particle release. Huh7.5.1 cells were infected with lentiviral vectors encoding an shRNA expression cassette of scrambled shRNA, shRNA-1, and shRNA-2. Four days after lentiviral infection, cells were infected with HCV (JFH1) at an MOI of 1. (A) Western blot analysis of HCV-infected cells with indicated shRNAs at day 6. IB, immunoblotting carried out using indicated antibodies. (B) Quantitative RT-PCR analysis of OSBP mRNA. (C) Quantitative RT-PCR analysis of GAPDH mRNA. (D) Intracellular HCV RNA levels measured by quantitative RT-PCR analysis. (E) Accumulation of extracellular HCV viral RNA in the culture medium as measured by quantitative RT-PCR analysis. (F) Supernatant infectivity assay. The infectivity of cultured supernatant at day 6 was determined as described in Materials and Methods and previously (58). Means and standard errors of at least triplicate measurements are shown. GE, genomic copies.

a base substitution mutation in the PH domain (W172A) (53), and mutation of FF to AA in the FFAT motif (FF/AA) (54) (Fig. 2B). Wild-type OSBP and the mutants were transiently transfected into Huh7 cells and analyzed for their subcellular distribution by indirect fluorescence microscopy using anti-FLAG antibody (OSBP and all OSBP mutants contain a FLAG tag at their N termini). Cells were counterstained with TGN46 antibody and DAPI. Both wild-type OSBP and the PH

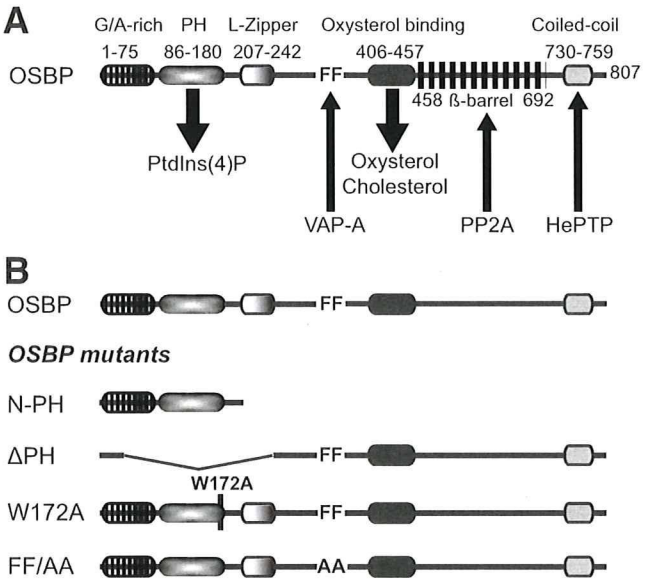

FIG. 2. Schematic representation of various OSBP domains. (A) The domain organizations of OSBP and amino acid regions are indicated on the figure. G/A-rich, glycine- and alanine-rich region; PH, binds to PI4P [PtdIns(4)P]; L-Zipper, leucine zipper domain; FF, FFAT; oxysterol-binding domain, binds to oxysterols and cholesterols. The numbering of amino acids is based on human OSBP (NM_002556). (B) OSBP mutants. The coding for the N-PH mutant extends from aa 1 to 208. The ΔPH mutant lacks aa 35 to 273. Mutant W172A carries a point mutation of a conserved tryptophan residue at 172 within the PH domain. Mutant FF/AA contains two phenylalanine residues in the FFAT motif replaced with alanine residues, required for VAP-A association. PP2A, phosphatase 2A; HePTP, tyrosine phosphatase.

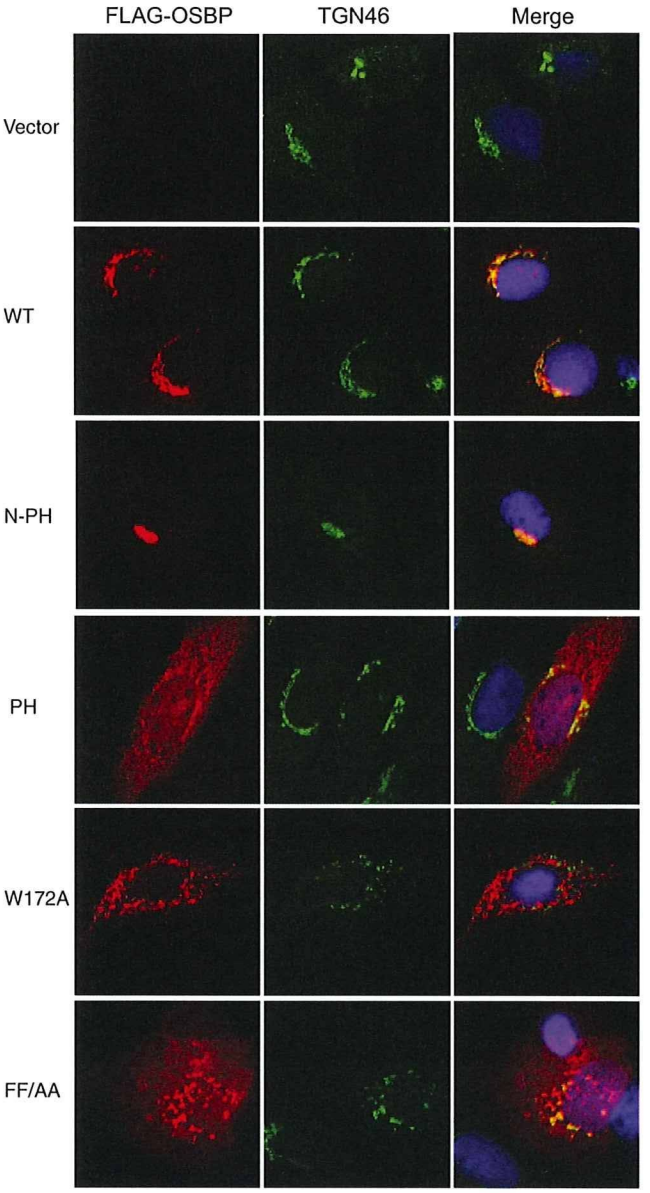

FIG. 3. Subcellular localization of OSBP and OSBP mutants. Huh7 cells were transfected with vectors encoding the FLAG-tagged wild-type (WT) and indicated mutant OSBP genes. Cells were analyzed by confocal immunofluorescence microscopy with anti-FLAG and anti-TGN46 antibodies (see Materials and Methods). Panels in the left column show FLAG-tagged OSBP (red). Panels in the center column show subcellular localization of TGN46 as a marker of the TGN. Panels in the right column show superimposed images of OSBP and TGN46.

domain-containing mutant (N-PH) predominantly localized to the Golgi compartment (Fig. 3). The N-PH mutant displayed Golgi compartment localizations as a consequence of its exposed PH domain. Other mutants including ΔPH and the base substitution mutants (W172A and FF/AA) in general displayed a diffuse cytosolic pattern of OSBP distribution. Both W172A and FF/AA mutants showed a punctate pattern of OSBP distribution in the cytosol and appeared to induce a distortion of TGN (Fig. 3). The OSBP mutant FF/AA displayed partial Golgi compartment localization. The substitutions of alanines for two phenylalanine residues in the FFAT motif abolish its ability to bind VAP-A (53, 54). VAP-A has been previously shown to bind NS5A (13, 17).

These OSBP mutants were also introduced into HCV-infected cells and examined for their effect on replication and viral particle release. Figure 4C shows a Western blot analysis of HCV-infected cells expressing ectopically expressed OSBP and its mutants. None of the OSBP mutants affected intracellular HCV RNA replication to any significant degree (Fig. 4B). However, the extracellular accumulation of viral RNA was affected by the ΔPH OSBP mutant (Fig. 4A). The PH domain is essential for the OSBP translocalization to the Golgi apparatus (24). Other mutants did not have any significant effect on the viral particle release except the W172A mutant. Surprisingly, the W172A mutant showed a modest increase in viral particle release. At present, we have no explanation for this observed result, but further characterization of this mutant will be needed. To further confirm the effect of OSBP mutants on HCV release, a chimeric HCV vector containing a luciferase reporter gene, analogous to Luc-Jc1 (23), was constructed and tested for virus production in the presence of OSBP mutants (Fig. 4D). Again, the ΔPH mutant consistently showed an inhibitory effect on viral particle release as assayed by luciferase activity of the released reporter virus. Based on these observations, the failure of the ΔPH OSBP mutant to maintain wild-type levels of viral particle release indicates that OSBP is

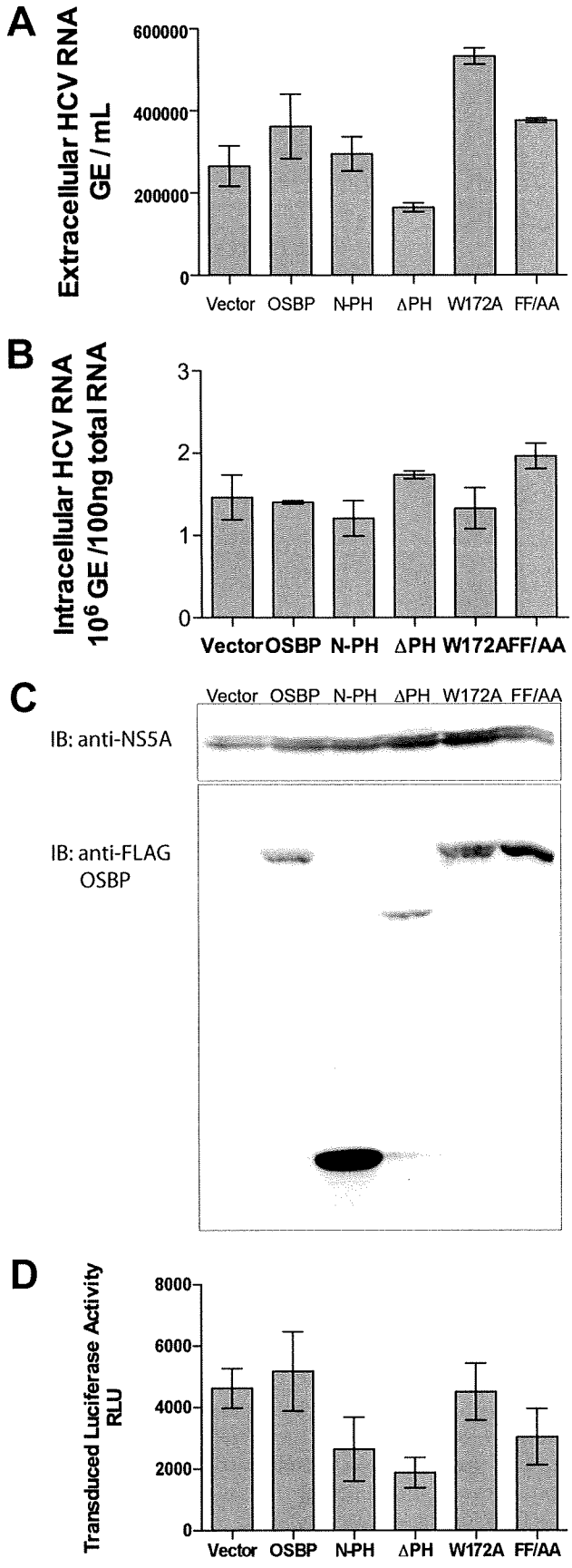

likely involved in viral particle release via the Golgi compartments.

NS5A binds OSBP. OSBP was identified in this study as an NS5A-associated protein (see Fig. S2C in the supplemental material). NS5A has been previously shown to interact with VAP-A and VAP-B (17). VAP-A also has been reported to bind OSBP (53). We have confirmed these interactions by immunoprecipitation studies. NS5A was shown to interact with OSBP and VAP-A (see Fig. S3A in the supplemental material). We further determined that OSBP interacts with NS5A irrespective of its genotypic origin. NS5A derived from genotype 1b (con1) or 2a (JFH1) binds to OSBP (see Fig. S3B in the supplemental material).

We next mapped the binding site(s) of OSBP within the NS5A protein. Huh7 cells were cotransfected with FLAG-tagged OSBP vector and various NS5A deletion mutants. All NS5A expression vectors contain a Myc/His tag (Fig. 5A). Cellular lysates were immunoprecipitated with anti-FLAG antibody to capture OSBP, followed by immunoblotting with anti-Myc antibody to probe for NS5A. Cellular lysates were examined for NS5A and OSBP expression by Western blot assays (Fig. 5B, upper and middle panels, respectively). The results show that N-terminal amino acid residues of NS5A in the region of amino acids (aa) 126 to 302 remained associated with OSBP (Fig. 5B, lower panel). These preliminary mapping studies identify domain I of NS5A as the approximate binding site(s) for OSBP. A more clearly defined motif of the NS5A region harboring OSBP binding needs to be identified. The interaction between NS5A and OSBP was also supported by the merged images of these proteins by confocal immunofluorescence microscopy, which displays a Golgi network-like pattern (see Fig. S4 in the supplemental material). The slightly diffuse pattern of OSBP seen here may reflect the state of the HCV-infected cell which may have contributed to the altered ER-Golgi apparatus pattern.

Oxysterol stimulates Golgi translocalization of OSBP and NS5A. 25-HC represents an oxidized sterol species and the most potent ligand for OSBP. The ligand binding to the OSBP triggers its Golgi translocalization, especially in the TGN. In Huh7 cells, the subcellular distribution of endogenous OSBP protein was cytosolic/vesicular as well as associated with the Golgi apparatus. OSBP association with the Golgi apparatus is seen as superimposed images in light blue (Fig. 6, top row).

FIG. 4. Effect of OSBP mutants on HCV replication and secretion. Huh7 cells were infected with HCV at an MOI of 0.5, maintained for 8 days, transfected with OSBP expression vector by electroporation, and analyzed after 48 h by RT-PCR (A and B) and Western blot assays (C). (A) Accumulation of HCV RNA in the culture supernatant. (B) The level of intracellular HCV RNA. (C) Western blot analysis of the HCV-infected cells using anti-NS5A (upper panel) and anti-FLAG for the detection of OSBP and mutants (lower panel). (D) Production of chimeric reporter HCV. Huh7.5.1 cells were transfected with both Luc-Jc1 RNA (luciferase reporter virus) and wild-type and mutant OSBP expression vectors, as indicated. Culture supernatants were collected at 72 h after transfection and used to infect naïve Huh7.5.1 cells. Cellular lysates from these secondary infections were assayed at 42 h for luciferase activity to determine the level of infectious reporter virion titer. Means and standard errors of at least triplicate measurements are shown. Expression vectors used for all the experiments are indicated. GE, genomic copies.

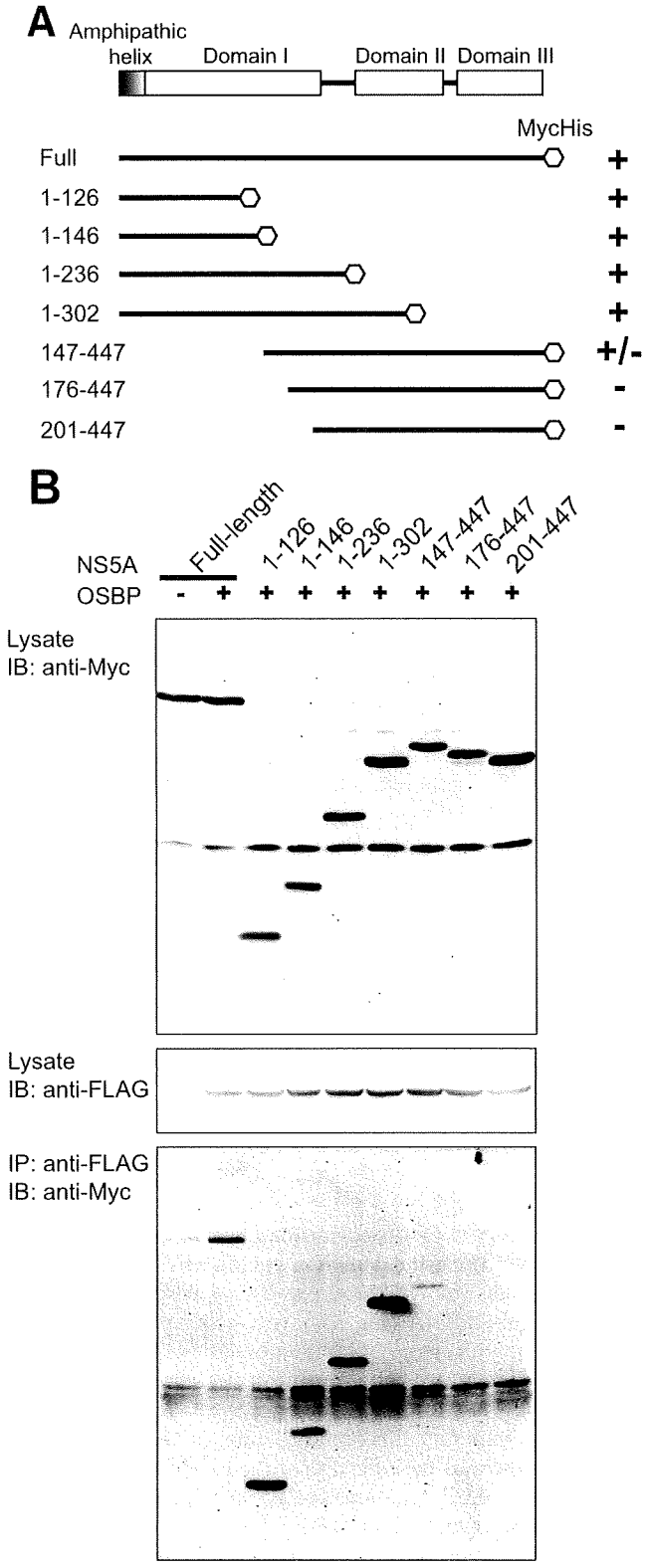

FIG. 5. Mapping of OSBP binding site(s) within the NS5A protein. (A) Schematic representation of wild-type and deletion mutants of NS5A encoded by pEF-NS5A vectors. Various domains of NS5A are shown. Huh7 cells were cotransfected with OSBP (pFLAG-CMV-OSBP), wild-type NS5A (pEF1-NS5A), or NS5A deletion mutants. Wild-type and mutant NS5A expression vectors contain a Myc/His tag. (B) Expression of wild-type NS5A, NS5A deletion mutant proteins (upper panel), and OSBP (middle panel) was analyzed by Western blot assays. For OSBP-NS5A protein-protein interaction studies, cellular lysates were immunoprecipitated (IP) using anti-FLAG antibody (OSBP), followed by immunoblotting (IB) using anti-Myc antibody (lower panel).

When Huh7 cells were stimulated by 25-HC, OSBP displayed a discrete and predominant Golgi compartment localization (Fig. 6, second row). When we analyzed the subcellular distribution of NS5A upon 25-HC stimulation in the HCV (JFH1)-infected cells, NS5A, in addition to its typical punctate ER localization, also displayed a discrete localization to the TGN. The merged image of OSBP and NS5A localization in the Golgi network can be seen in yellow (Fig. 6, bottom row).

We also examined this phenomenon in cells expressing the NS5A gene via an ectopic expression vector encoding NS5A. As can be seen, the addition of 25-HC again triggered its Golgi compartment distribution, suggesting that NS5A via its interaction with OSBP is targeted to the Golgi compartment (see Fig. S4B in the supplemental material). This result suggests that NS5A can localize to the Golgi compartment in the absence of other viral proteins or without the context of HCV infection. These associations clearly implicate NS5A's involvement in the HCV maturation/release processes.

DISCUSSION

HCV RNA replicates within a RNP complex in the modified membranous structures originated from the ER. Lipid droplets and rafts have been implicated in supporting HCV replication (13, 28). Host lipid synthesis has been shown to play an essential role in the viral reproduction process (40). Several inhibitors of lipid/fatty acid biosynthesis affect viral RNA synthesis and most likely the secretion of HCV. Our proteomic analysis of HCV viral protein complexes revealed the association of OSBP along with other factors involved in lipid/fatty acid biosynthetic pathways. Here, we investigated the functional role of OSBP in HCV replication and postreplicative processes. OSBP, a cytosolic lipid binding protein that translocates to the Golgi compartment upon ligand binding, plays a functional role in the ER to Golgi lipid trafficking.

VAP-A, which has been previously shown to bind viral proteins NS5A and NS5B, has emerged as a key player in this process. VAP-A, which is mostly localized in the ER, is known to interact with both OSBP and CERT thorough the FFAT motif, a motif shared by these lipid-binding proteins. It is interesting that the NS5A staining pattern with VAP-A and OSBP mirrors the distribution of these cellular proteins in the merged images (see Fig. S4A in the supplemental material). Both CERT and OSBP proteins contain the PH domain and are targeted to the Golgi apparatus and interact with each other at the ER-Golgi membrane contact sites (35, 36). PI transported to the Golgi compartment by Nir-2 is phosphorylated in the Golgi compartment by PI4 kinase, producing PI4P, which recruits OSBP and CERT by direct binding to their PH domains (35). Through these actions, CERT then transfers ceramide from the ER to the Golgi apparatus, which enables the production of sphingomyelin (SM) and diacylglycerol in the TGN. These studies establish the functional role of OSBP in regulation of lipid trans-

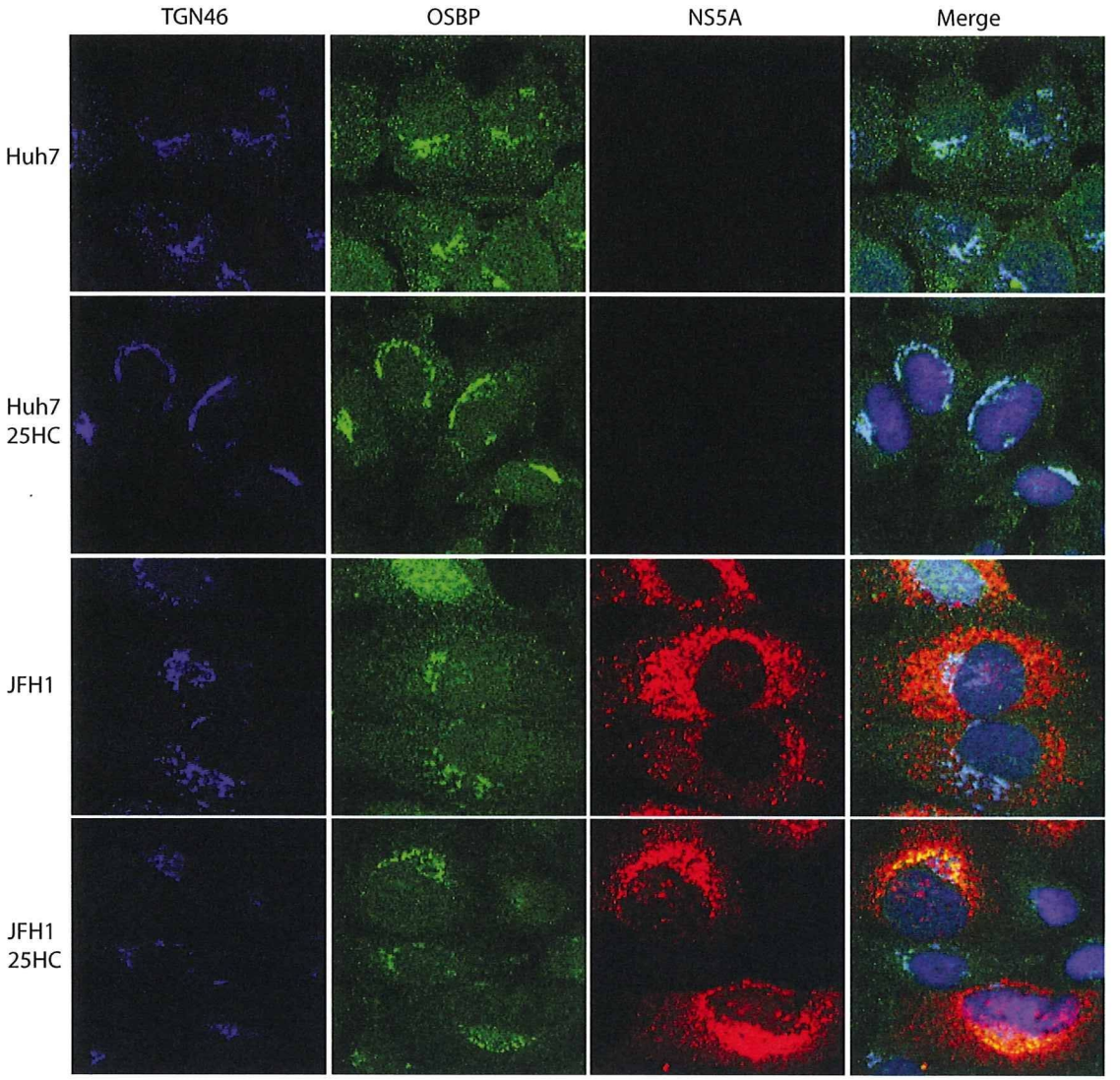

FIG. 6. 25-HC stimulates Golgi compartment localization of OSBP and NS5A. Uninfected and HCV (JFH1)-infected Huh7 cells were treated with or without 10 μM 25-HC and incubated for 12 h prior to immunostaining. The immunofluorescence assay was performed as described in Materials and Methods.

port from the ER to the Golgi apparatus and stimulation of SM synthesis. In this context, a recent study showed that HPA-12, an inhibitor SM synthesis, blocked HCV secretion, thus lending support to the model that HCV maturation/secretion may be occurring through the Golgi compartment (2). In this respect, two recent reports have demonstrated an indispensable role of PI4 kinases in HCV replication (4, 42).

Using RNA interference studies, it is shown that partial depletion of OSBP did not affect HCV replication but dramatically inhibited the accumulation of HCV particles (Fig. 1B to E). OSBP-specific shRNA-1, which severely depleted OSBP protein, affected both viral RNA replication and virion secretion. Such a depletion of OSBP by shRNA-1 also affected viral gene expression (Fig. 1A), suggesting that OSBP may be involved in the regulation of viral gene expression (translation/replication). The exact mechanism(s) by which this may occur remains to be characterized. Complete depletion of OSBP has been shown to cause Golgi apparatus fragmentation and inhibition of transport of vesicular stomatitis virus glycoprotein from the ER (30). Partial depletion of OSBP by shRNA-2 gave different results. The viral gene expression was proportionally affected by this shRNA (Fig. 1A). Intracellular levels of viral RNA were not affected, but the accumulation of extracellular RNA was severely reduced. This result suggested the involvement of OSBP in virion secretion.

Mutations within the functional domains of OSBP that affect its various functions have been described (50). We developed a few of these OSBP mutations and ectopically expressed them in HCV-infected cells (Fig. 2B). Most of these mutations displayed diffuse patterns of OSBP with reduced Golgi compartment localizations (W172A and FF/AA). The PH domain deletion mutant, ΔPH, failed to localize to the Golgi compartment, impairing the virion release (Fig. 1D and E). Overall, results of this study point more emphatically to a major role of OSBP in the regulation of virion secretion.

Several studies support the notion that HCV may utilize the

VLDL secretory pathway (6, 14, 19, 29). The most compelling evidence comes from the use of microsomal transfer protein inhibitor and ApoB silencing studies, both of which affect the VLDL particle assembly (14). Microsomal transfer protein inhibitor and ApoB small interfering RNA affect the accumulation of extracellular viral RNA while not affecting intracellular viral RNA replication (14). Use of the antioxidant flavonoid naringenin, which inhibits VLDL assembly, similarly inhibited virion release (29). Huang and colleagues showed that secretion of HCV infectious particles is dependent on active secretion of VLDL, showing that the VLDL assembly/secretion pathway is being utilized by HCV (19). Pre-VLDL particles are assembled in the ER, and mature VLDL particle formation occurs in the Golgi apparatus (16). While it is not known whether OSBP localization and/or trafficking to the Golgi apparatus is needed for VLDL secretion, we show here that NS5A along with OSBP is localized to the Golgi apparatus as well as to its characteristic localization in the ER. Our confocal microscopy studies show that a notable fraction of NS5A is localized to the Golgi compartment (Fig. 6). These data implicate a pivotal role of NS5A in a virion maturation process, which likely occurs in the Golgi compartments. NS5A interacts with OSBP via its N-terminal residues, and this interaction may be needed for NS5A's localization to the Golgi compartment as well. The preliminary data presented here map the binding site(s) of OSBP within domain I of NS5A (Fig. 4). Exact motifs involved in this interaction remain to be characterized. NS5A has three functional domains (I, II, and III). Domains I and II are relevant to the regulation of HCV RNA replication. Several studies point to the role of domain III in HCV particle secretion (3, 27, 45). The serine 457 residue in this domain, in particular, which is also the site of casein kinase II phosphorylation, has been shown to be essential for virion production (45). It will be of interest to determine the Golgi localization of an NS5A Ser^{457} mutant. The importance of Golgi trafficking for the HCV life cycle is further supported by the observations that HCV envelope proteins traffic thorough the cisternae of the Golgi compartment for glycosylation (32). Little is known about the HCV assembly and secretion processes. The studies described herein represent attempts to probe into these processes. Clearly, the delineation of these pathways is needed for the elucidation of the HCV life cycle and its relevance to infectious processes.

In summary, we have demonstrated that OSBP function(s) is relevant to the HCV maturation process. Our studies also suggest that NS5A localizes to the Golgi compartment and that OSBP and NS5A together aid in the viral assembly and or secretion processes. Further studies are needed to characterize, in depth, the exact role(s) of OSBP in the various steps of the HCV life cycle.

ACKNOWLEDGMENTS

We thank T. Wakita for the generous gift of the infectious JFH1 molecular clone and the subgenomic construct, F. Chisari (Scripps Research Institute, La Jolla, CA) for the kind gift of Huh7.5.1 cells, C. Rice and C. Cameron for anti-NS5A antibodies, I. Verma (Salk Institute, La Jolla, CA) for providing lentiviral plasmids, and Y. Matsuura for providing VAP-A expression vector.

This study was supported by NIH grants DK077704 and U19066313 to A.S. and P41 RR011823 to J.Y.

REFERENCES

1. **Ahlquist, P., A. O. Noueiry, W. M. Lee, D. B. Kushner, and B. T. Dye.** 2003. Host factors in positive-strand RNA virus genome replication. J. Virol. **77**:8181–8186.
2. **Aizaki, H., K. Morikawa, M. Fukasawa, H. Hara, Y. Inoue, H. Tani, K. Saito, M. Nishijima, K. Hanada, Y. Matsuura, M. M. Lai, T. Miyamura, T. Wakita, and T. Suzuki.** 2008. Critical role of virion-associated cholesterol and sphingolipid in hepatitis C virus infection. J. Virol. **82**:5715–5724.
3. **Appel, N., M. Zayas, S. Miller, J. Krijnse-Locker, T. Schaller, P. Friebe, S. Kallis, U. Engel, and R. Bartenschlager.** 2008. Essential role of domain III of nonstructural protein 5A for hepatitis C virus infectious particle assembly. PLoS Pathog. **4**:e1000035.
4. **Berger, K. L., J. D. Cooper, N. S. Heaton, R. Yoon, T. E. Oakland, T. X. Jordan, G. Mateu, A. Grakoui, and G. Randall.** 2009. Roles for endocytic trafficking and phosphatidylinositol 4-kinase III alpha in hepatitis C virus replication. Proc. Natl. Acad. Sci. USA **106**:7577–7582.
5. **Bern, M., D. Goldberg, W. H. McDonald, and J. R. Yates, 3rd.** 2004. Automatic quality assessment of peptide tandem mass spectra. Bioinformatics **20**(Suppl. 1):i49–i54.
6. **Chang, K. S., J. Jiang, Z. Cai, and G. Luo.** 2007. Human apolipoprotein e is required for infectivity and production of hepatitis C virus in cell culture. J. Virol. **81**:13783–13793.
7. **Chomczynski, P., and N. Sacchi.** 2006. The single-step method of RNA isolation by acid guanidinium thiocyanate-phenol-chloroform extraction: twenty-something years on. Nat. Protoc. **1**:581–585.
8. **Cociorva, D., L. T. D., and J. R. Yates.** 2007. Validation of tandem mass spectrometry database search results using DTASelect. Curr. Protoc. Bioinformatics Chapter **13**:Unit 13.4.
9. **Diop, S. B., K. Bertaux, D. Vasanthi, A. Sarkeshik, B. Goirand, D. Aragnol, N. S. Tolwinski, M. D. Cole, J. Pradel, J. R. Yates III, R. K. Mishra, Y. Graba, and A. J. Saurin.** 2008. Reptin and pontin function antagonistically with PcG and TrxG complexes to mediate Hox gene control. EMBO Rep. **9**:260–266.
10. **Elazar, M., K. H. Cheong, P. Liu, H. B. Greenberg, C. M. Rice, and J. S. Glenn.** 2003. Amphipathic helix-dependent localization of NS5A mediates hepatitis C virus RNA replication. J. Virol. **77**:6055–6061.
11. **Eng, J., A. McCormack, and J. R. Yates, 3rd.** 1994. An approach to correlate tandem mass spectral data of peptides with amino acid sequences in a protein database. J. Am. Soc. Mass Spectrom. **5**:976–989.
12. **Evans, M. J., C. M. Rice, and S. P. Goff.** 2004. Phosphorylation of hepatitis C virus nonstructural protein 5A modulates its protein interactions and viral RNA replication. Proc. Natl. Acad. Sci. USA **101**:13038–13043.
13. **Gao, L., H. Aizaki, J. W. He, and M. M. Lai.** 2004. Interactions between viral nonstructural proteins and host protein hVAP-33 mediate the formation of hepatitis C virus RNA replication complex on lipid raft. J. Virol. **78**:3480–3488.
14. **Gastaminza, P., G. Cheng, S. Wieland, J. Zhong, W. Liao, and F. V. Chisari.** 2008. Cellular determinants of hepatitis C virus assembly, maturation, degradation, and secretion. J. Virol. **82**:2120–2129.
15. **Gosert, R., D. Egger, V. Lohmann, R. Bartenschlager, H. E. Blum, K. Bienz, and D. Moradpour.** 2003. Identification of the hepatitis C virus RNA replication complex in Huh-7 cells harboring subgenomic replicons. J. Virol. **77**:5487–5492.
16. **Gusarova, V., J. Seo, M. L. Sullivan, S. C. Watkins, J. L. Brodsky, and E. A. Fisher.** 2007. Golgi-associated maturation of very low density lipoproteins involves conformational changes in apolipoprotein B, but is not dependent on apolipoprotein E. J. Biol. Chem. **282**:19453–19462.
17. **Hamamoto, I., Y. Nishimura, T. Okamoto, H. Aizaki, M. Liu, Y. Mori, T. Abe, T. Suzuki, M. M. Lai, T. Miyamura, K. Moriishi, and Y. Matsuura.** 2005. Human VAP-B is involved in hepatitis C virus replication through interaction with NS5A and NS5B. J. Virol. **79**:13473–13482.
18. **Huang, H., Y. Chen, and J. Ye.** 2007. Inhibition of hepatitis C virus replication by peroxidation of arachidonate and restoration by vitamin E. Proc. Natl. Acad. Sci. USA **104**:18666–18670.
19. **Huang, H., F. Sun, D. M. Owen, W. Li, Y. Chen, M. Gale, Jr., and J. Ye.** 2007. Hepatitis C virus production by human hepatocytes dependent on assembly and secretion of very low-density lipoproteins. Proc. Natl. Acad. Sci. USA **104**:5848–5853.
20. **Inubushi, S., M. Nagano-Fujii, K. Kitayama, M. Tanaka, C. An, H. Yokozaki, H. Yamamura, H. Nuriya, M. Kohara, K. Sada, and H. Hotta.** 2008. Hepatitis C virus NS5A protein interacts with and negatively regulates the non-receptor protein tyrosine kinase Syk. J. Gen. Virol. **89**:1231–1242.
21. **Kapadia, S. B., and F. V. Chisari.** 2005. Hepatitis C virus RNA replication is regulated by host geranylgeranylation and fatty acids. Proc. Natl. Acad. Sci. USA **102**:2561–2566.
22. **Kato, T., T. Date, M. Miyamoto, M. Sugiyama, Y. Tanaka, E. Orito, T. Ohno, K. Sugihara, I. Hasegawa, K. Fujiwara, K. Ito, A. Ozasa, M. Mizokami, and T. Wakita.** 2005. Detection of anti-hepatitis C virus effects of interferon and ribavirin by a sensitive replicon system. J. Clin. Microbiol. **43**:5679–5684.
23. **Koutsoudakis, G., A. Kaul, E. Steinmann, S. Kallis, V. Lohmann, T. Pietschmann, and R. Bartenschlager.** 2006. Characterization of the early steps

of hepatitis C virus infection by using luciferase reporter viruses. J. Virol. **80:**5308–5320.
24. **Lagace, T. A., D. M. Byers, H. W. Cook, and N. D. Ridgway.** 1997. Altered regulation of cholesterol and cholesteryl ester synthesis in Chinese-hamster ovary cells overexpressing the oxysterol-binding protein is dependent on the pleckstrin homology domain. Biochem. J. **326:**205–213.
25. **Levine, T. P., and S. Munro.** 2002. Targeting of Golgi-specific pleckstrin homology domains involves both PtdIns 4-kinase-dependent and -independent components. Curr. Biol. **12:**695–704.
26. **MacCoss, M. J., C. C. Wu, and J. R. Yates, 3rd.** 2002. Probability-based validation of protein identifications using a modified SEQUEST algorithm. Anal. Chem. **74:**5593–5599.
27. **Masaki, T., R. Suzuki, K. Murakami, H. Aizaki, K. Ishii, A. Murayama, T. Date, Y. Matsuura, T. Miyamura, T. Wakita, and T. Suzuki.** 2008. Interaction of hepatitis C virus nonstructural protein 5A with core protein is critical for the production of infectious virus particles. J. Virol. **82:**7964–7976.
28. **Miyanari, Y., K. Atsuzawa, N. Usuda, K. Watashi, T. Hishiki, M. Zayas, R. Bartenschlager, T. Wakita, M. Hijikata, and K. Shimotohno.** 2007. The lipid droplet is an important organelle for hepatitis C virus production. Nat. Cell Biol. **9:**1089–1097.
29. **Nahmias, Y., J. Goldwasser, M. Casali, D. van Poll, T. Wakita, R. T. Chung, and M. L. Yarmush.** 2008. Apolipoprotein B-dependent hepatitis C virus secretion is inhibited by the grapefruit flavonoid naringenin. Hepatology **47:**1437–1445.
30. **Ngo, M., and N. D. Ridgway.** 2009. Oxysterol binding protein (OSBP)-related protein 9 (ORP9) is a cholesterol transfer protein that regulates Golgi structure and function. Mol. Biol. Cell **20:**1388–1399.
31. **Nishimura, T., T. Inoue, N. Shibata, A. Sekine, W. Takabe, N. Noguchi, and H. Arai.** 2005. Inhibition of cholesterol biosynthesis by 25-hydroxycholesterol is independent of OSBP. Genes Cells **10:**793–801.
32. **Op De Beeck, A., C. Voisset, B. Bartosch, Y. Ciczora, L. Cocquerel, Z. Keck, S. Foung, F. L. Cosset, and J. Dubuisson.** 2004. Characterization of functional hepatitis C virus envelope glycoproteins. J. Virol. **78:**2994–3002.
33. **Pawlotsky, J. M.** 2004. Pathophysiology of hepatitis C virus infection and related liver disease. Trends Microbiol. **12:**96–102.
34. **Peng, J., J. E. Elias, C. C. Thoreen, L. J. Licklider, and S. P. Gygi.** 2003. Evaluation of multidimensional chromatography coupled with tandem mass spectrometry (LC/LC-MS/MS) for large-scale protein analysis: the yeast proteome. J. Proteome Res. **2:**43–50.
35. **Peretti, D., N. Dahan, E. Shimoni, K. Hirschberg, and S. Lev.** 2008. Coordinated lipid transfer between the endoplasmic reticulum and the Golgi complex requires the VAP proteins and is essential for Golgi-mediated transport. Mol. Biol. Cell **19:**3871–3884.
36. **Perry, R. J., and N. D. Ridgway.** 2006. Oxysterol-binding protein and vesicle-associated membrane protein-associated protein are required for sterol-dependent activation of the ceramide transport protein. Mol. Biol. Cell **17:**2604–2616.
37. **Randall, G., M. Panis, J. D. Cooper, T. L. Tellinghuisen, K. E. Sukhodolets, S. Pfeffer, M. Landthaler, P. Landgraf, S. Kan, B. D. Lindenbach, M. Chien, D. B. Weir, J. J. Russo, J. Ju, M. J. Brownstein, R. Sheridan, C. Sander, M. Zavolan, T. Tuschl, and C. M. Rice.** 2007. Cellular cofactors affecting hepatitis C virus infection and replication. Proc. Natl. Acad. Sci. USA **104:** 12884–12889.
38. **Ridgway, N. D., P. A. Dawson, Y. K. Ho, M. S. Brown, and J. L. Goldstein.** 1992. Translocation of oxysterol binding protein to Golgi apparatus triggered by ligand binding. J. Cell Biol. **116:**307–319.
39. **Sadygov, R. G., J. Eng, E. Durr, A. Saraf, H. McDonald, M. J. MacCoss, and J. R. Yates III.** 2002. Code developments to improve the efficiency of automated MS/MS spectra interpretation. J. Proteome Res. **1:**211–215.
40. **Su, A. I., J. P. Pezacki, L. Wodicka, A. D. Brideau, L. Supekova, R. Thimme, S. Wieland, J. Bukh, R. H. Purcell, P. G. Schultz, and F. V. Chisari.** 2002. Genomic analysis of the host response to hepatitis C virus infection. Proc. Natl. Acad. Sci. USA **99:**15669–15674.
41. **Tabb, D. L., W. H. McDonald, and J. R. Yates III.** 2002. DTASelect and Contrast: tools for assembling and comparing protein identifications from shotgun proteomics. J. Proteome Res. **1:**21–26.
42. **Tai, A. W., Y. Benita, L. F. Peng, S. S. Kim, N. Sakamoto, R. J. Xavier, and R. T. Chung.** 2009. A functional genomic screen identifies cellular cofactors of hepatitis C virus replication. Cell Host Microbe **5:**298–307.
43. **Takeuchi, T., A. Katsume, T. Tanaka, A. Abe, K. Inoue, K. Tsukiyama-Kohara, R. Kawaguchi, S. Tanaka, and M. Kohara.** 1999. Real-time detection system for quantification of hepatitis C virus genome. Gastroenterology **116:**636–642.
44. **Targett-Adams, P., S. Boulant, and J. McLauchlan.** 2008. Visualization of double-stranded RNA in cells supporting hepatitis C virus RNA replication. J. Virol. **82:**2182–2195.
45. **Tellinghuisen, T. L., K. L. Foss, and J. Treadaway.** 2008. Regulation of hepatitis C virion production via phosphorylation of the NS5A protein. PLoS Pathog **4:**e1000032.
46. **Tiscornia, G., O. Singer, and I. M. Verma.** 2006. Design and cloning of lentiviral vectors expressing small interfering RNAs. Nat. Protoc. **1:**234–240.
47. **van den Hoff, M. J., A. F. Moorman, and W. H. Lamers.** 1992. Electroporation in "intracellular" buffer increases cell survival. Nucleic Acids Res. **20:**2902.
48. **Wakita, T., T. Pietschmann, T. Kato, T. Date, M. Miyamoto, Z. Zhao, K. Murthy, A. Habermann, H. G. Krausslich, M. Mizokami, R. Bartenschlager, and T. J. Liang.** 2005. Production of infectious hepatitis C virus in tissue culture from a cloned viral genome. Nat. Med. **11:**791–796.
49. **Wang, P. Y., J. Weng, and R. G. Anderson.** 2005. OSBP is a cholesterol-regulated scaffolding protein in control of ERK 1/2 activation. Science **307:** 1472–1476.
50. **Wang, P. Y., J. Weng, S. Lee, and R. G. Anderson.** 2008. The N terminus controls sterol binding while the C terminus regulates the scaffolding function of OSBP. J. Biol. Chem. **283:**8034–8045.
51. **Waris, G., D. J. Felmlee, F. Negro, and A. Siddiqui.** 2007. Hepatitis C virus induces proteolytic cleavage of sterol regulatory element binding proteins and stimulates their phosphorylation via oxidative stress. J. Virol. **81:**8122–8130.
52. **Waris, G., J. Turkson, T. Hassanein, and A. Siddiqui.** 2005. Hepatitis C virus (HCV) constitutively activates STAT-3 via oxidative stress: role of STAT-3 in HCV replication. J. Virol. **79:**1569–1580.
53. **Wyles, J. P., C. R. McMaster, and N. D. Ridgway.** 2002. Vesicle-associated membrane protein-associated protein-A (VAP-A) interacts with the oxysterol-binding protein to modify export from the endoplasmic reticulum. J. Biol. Chem. **277:**29908–29918.
54. **Wyles, J. P., and N. D. Ridgway.** 2004. VAMP-associated protein-A regulates partitioning of oxysterol-binding protein-related protein-9 between the endoplasmic reticulum and Golgi apparatus. Exp. Cell Res. **297:**533–547.
55. **Yan, D., and V. M. Olkkonen.** 2008. Characteristics of oxysterol binding proteins. Int. Rev. Cytol. **265:**253–285.
56. **Ye, J.** 2007. Reliance of host cholesterol metabolic pathways for the life cycle of hepatitis C virus. PLoS Pathog. **3:**e108.
57. **Ye, J., C. Wang, R. Sumpter, Jr., M. S. Brown, J. L. Goldstein, and M. Gale, Jr.** 2003. Disruption of hepatitis C virus RNA replication through inhibition of host protein geranylgeranylation. Proc. Natl. Acad. Sci. USA **100:**15865–15870.
58. **Zhong, J., P. Gastaminza, G. Cheng, S. Kapadia, T. Kato, D. R. Burton, S. F. Wieland, S. L. Uprichard, T. Wakita, and F. V. Chisari.** 2005. Robust hepatitis C virus infection in vitro. Proc. Natl. Acad. Sci. USA **102:**9294–9299.

JOURNAL OF VIROLOGY, Oct. 2009, p. 9993–10006 Vol. 83, No. 19
0022-538X/09/$08.00+0 doi:10.1128/JVI.00509-09

The Hepatitis C Virus Core Protein Contains a BH3 Domain That Regulates Apoptosis through Specific Interaction with Human Mcl-1▽†

Nur Khairiah Mohd-Ismail,[1,2] Lin Deng,[3] Sunil Kumar Sukumaran,[4] Victor C. Yu,[4,5] Hak Hotta,[3] and Yee-Joo Tan[1]*

Collaborative Anti-Viral Research Group, Institute of Molecular and Cell Biology, Singapore[1]; NUS Graduate School for Integrative Sciences and Engineering, Singapore[2]; Division of Microbiology, Kobe University Graduate School of Medicine, Kobe, Japan[3]; Mechanisms of Apoptosis in Mammalian Cell Group, Institute of Molecular and Cell Biology, Singapore[4]; and Department of Pharmacy, Faculty of Science, National University of Singapore, Singapore[5]

Received 11 March 2009/Accepted 8 July 2009

The hepatitis C virus (HCV) core protein is known to modulate apoptosis and contribute to viral replication and pathogenesis. In this study, we have identified a Bcl-2 homology 3 (BH3) domain in the core protein that is essential for its proapoptotic property. Coimmunoprecipitation experiments showed that the core protein interacts specifically with the human myeloid cell factor 1 (Mcl-1), a prosurvival member of the Bcl-2 family, but not with other prosurvival members (Bcl-X_L and Bcl-w). Moreover, the overexpression of Mcl-1 protects against core-induced apoptosis. By using peptide mimetics, core was found to release cytochrome *c* from isolated mitochondria when complemented with Bad. Thus, core is a bona fide BH3-only protein having properties similar to those of Noxa, a BH3-only member of the Bcl-2 family that binds preferentially to Mcl-1. There are three critical hydrophobic residues in the BH3 domain of the core protein, and they are essential for the proapoptotic property of the core protein. Furthermore, the genotype 1b core protein is more effective than the genotype 2a core protein in inducing apoptosis due to a single-amino-acid difference at one of these hydrophobic residues (residue 119). Replacing this residue in the J6/JFH-1 infectious clone (genotype 2a) with the corresponding amino acid in the genotype 1b core protein produced a mutant virus, J6/JFH-1(V119L), which induced significantly higher levels of apoptosis in the infected cells than the parental J6/JFH-1 virus. Furthermore, the core protein of J6/JFH-1(V119L), but not that of J6/JFH-1, interacted with Mcl-1 in virus-infected cells. Taken together, the core protein is a novel BH3-only viral homologue that contributes to the induction of apoptosis during HCV infection.

Hepatitis C virus (HCV), a positive-stranded RNA virus of the family *Flaviviridae*, is the major cause of non-A, non-B hepatitis worldwide. The HCV genome encodes a precursor polyprotein of ~3,000 amino acids (aa) that is processed cotranslationally and posttranslationally to give rise to viral structural and nonstructural proteins (2). The core protein is encoded by the N-terminal portion of the HCV precursor polyprotein and cleaved from the polyprotein by cellular signal peptidase to give the immature form of the core protein (aa 1 to 191). This then is further cleaved by membrane-associated signal peptide peptidase to give the mature core protein, whose C terminus is not precisely known but lies between residues 170 and 179 (see reviews in references 33, 42, and 52). The mature core protein is thought to constitute the HCV capsid and is the predominant form detected in virus particles purified from the sera of patients with chronic HCV infection (42, 74). A recent paper also reported that the maturation of the core protein is required for the production of HCV using the JFH-1 infectious clone (65).

Besides its role in the encapsidation of viral RNA, the core protein has been found to interfere with many cellular pathways, including cell signaling, transcriptional activation, lipid metabolism, carcinogenesis, and apoptosis (see reviews in references 33, 42, and 52). As the regulation of apoptosis during viral infection is an important determinant in the struggle between virus and host for survival, many viruses encode viral proteins that can regulate apoptosis in the infected host cells and manipulate this process to their advantage. In the case of HCV, the mechanisms by which the virus maintains viral persistence and promotes hepatocellular carcinoma are not well understood, but several HCV proteins have the ability to modulate apoptosis (see recent reviews in references 20 and 28). In particular, the core protein has been shown to modulate apoptosis, and it seems that the core protein can inhibit as well as promote apoptosis, depending on the death stimuli and types of cells used (3, 9, 13, 25, 36, 40, 49, 53, 54, 57, 60, 76).

In this study, we characterized one of the mechanisms by which the mature form of the core protein from a genotype 1b strain induces apoptosis in Huh7 cells. Following the experimental designs used in previous studies (29, 38, 40, 55, 72), the mature form of the core protein is assumed to be constituted by residues 1 to 173 of the HCV precursor polyprotein, and

* Corresponding author. Mailing address: Cancer and Developmental Cell Biology Division, Institute of Molecular and Cell Biology, 61 Biopolis Drive, A*STAR (Agency for Science, Technology and Research), Biopolis, Singapore 136873, Singapore. Phone: 65-65869625. Fax: 65-67791117. E-mail: mcbtanyj@imcb.a-star.edu.sg.

† Supplemental material for this article may be found at http://jvi.asm.org/.

▽ Published ahead of print on 15 July 2009.

this shall be referred to as the core protein in this study. Here, we demonstrate that the core protein contains a functional Bcl-2 homology 3 (BH3) domain that is essential for its proapoptotic property and ability to interact with human myeloid cell factor 1 (Mcl-1), a prosurvival member of the Bcl-2 family (31). Detailed molecular analysis and infection studies using the J6/JFH-1 infectious clone showed that the core protein is a bona fide BH3-only protein that contributes to the induction of apoptosis during HCV infection by mimicking Noxa and interfering with the prosurvival function of Mcl-1.

MATERIALS AND METHODS

Construction of plasmids. Expression plasmids for the wild-type core protein and mutants were generated by PCR using Titanium *Taq* DNA polymerase (Clontech Laboratories Inc., Palo Alto, CA). Two plasmids containing full-length HCV genomes were used as templates. The first one is a 1b strain cloned in Singapore (59), and the second is the JFH-1 clone, which is a 2a strain (68). All sequences were confirmed by sequencing performed by the core facilities at the Institute of Molecular and Cell Biology, Singapore. The pXJ40flag vector is used so that a flag epitope is fused to the N terminus of the core protein, and this allows the comparison of protein expression levels with an anti-flag antibody.

Transient transfections, CaspACE fluorometric assay, and Western blot analysis. Transient transfections of Huh7 cells were performed using Lipofectamine reagent (Invitrogen, Carlsbad, CA) according to the manufacturer's protocol. Approximately 16 h after transfection, the activation of caspase-3 was quantified by using a CaspACE fluorometric assay system from Promega Corporation (Madison, WI) as previously described (63).

Western blot analysis was performed as previously described (64). The primary antibodies (anti-myc monoclonal and anti-myc and anti-Mcl-1 polyclonal [Santa Cruz Biotechnology, Santa Cruz, CA], anti-Mcl-1 monoclonal [Calbiochem, La Jolla, CA], anti-actin monoclonal, anti-Hsp-60 monoclonal, anti-flag monoclonal and polyclonal [Sigma, St. Louis, MO], anti-poly[ADP-ribose] polymerase [PARP] polyclonal [Cell Signaling Technology Inc., Beverly, MA], anti-cytochrome *c* monoclonal [BD PharMingen, BD Biosciences, San Jose, CA], and anti-Noxa [Imgenex, San Diego, CA]) were purchased. Anti-core protein monoclonal antibody (clone 2H9; a kind gift from T. Wakita, Department of Virology II, National Institute of Infectious Diseases, Tokyo, Japan) was used to detect the core protein of HCV (68).

Coimmunoprecipitation experiments. For the coimmunoprecipitation experiments, each 6-cm dish of cells was resuspended in 200 μl of immunoprecipitation (IP) buffer (50 mM Tris-HCl, pH 8, 150 mM NaCl, 0.5% NP-40, 0.5% deoxycholic acid, 0.005% sodium dodecyl sulfate [SDS], and 1 mM phenylmethylsulfonyl fluoride) and subjected to freeze-thawing six times. Anti-flag monoclonal antibody conjugated to Sepharose beads (Sigma) were added to 150 μl of the lysates, and the mixture was subjected to end-over-end mixing at 4°C for 6 h. Beads were washed four times with cold IP buffer, and then 15 μl of Laemmli's SDS buffer was added and the samples were boiled at 100°C for 5 min to release the immunocomplexes. Samples were separated by SDS-polyacrylamide gel electrophoresis and subjected to Western blot analysis.

Alternatively, rabbit anti-Mcl-1 polyclonal antibody was used to immunoprecipitate endogenous Mcl-1 protein. In this case, 7 μg of antibody (either anti-Mcl-1 or anti-hemagglutinin [HA] polyclonal antibody [Santa Cruz Biotechnology]) was added to the lysates obtained from two dishes of cells and allowed to mix for 1 h at room temperature. Protein A agarose beads (Roche, Indianapolis, IN) were added, and the mixture was subjected to end-over-end mixing at 4°C overnight. The coimmunoprecipitated proteins then were detected as described above.

Quantification of autoradiographs. An imaging densitometer (Bio-Rad, Hercules, CA) was used for the quantification of the intensities of specific bands on autoradiographs.

In vitro cytochrome *c* release assay. For the in vitro cytochrome *c* release assays, mitochondria were isolated from 293T cells as previously described (22). Briefly, 293T cells were suspended in isolation buffer (320 mM sucrose, 1 mM EDTA, 50 mM HEPES [pH 7.5]) and disrupted by 25 expulsions through a 27-gauge needle. The disrupted cells were spun at 1,000 × *g* for 10 min to remove cell debris and nuclei. The supernatant was centrifuged at 7,000 × *g* for 10 min, and the pellet was retained as the heavy membrane fraction containing the mitochondria. The mitochondrion-containing pellets then were resuspended in assay buffer (250 mM sucrose, 2 mM KH_2PO_4, 5 mM sodium succinate, 25 mM EGTA, and 10 mM HEPES [pH 7.5]) at 0.5 mg/ml. Equal amounts of mitochondria were treated with the indicated peptides for 30 min at room temperature, followed by centrifugation. Both the supernatant and pellet then were subjected to SDS-polyacrylamide gel electrophoresis, followed by Western blot analysis to determine the amount of cytochrome *c* released from the mitochondria. Hsp-60 was used as a loading control for the pellet.

Synthesis of peptides. A peptide that corresponds to residues 118 to 149 of the genotype 1b core protein (NLGKVIDTLTCGFADLMGYIPLVGAPLGG AAR) was synthesized and purified to 95% purity (Sigma Genosys, Japan). Peptides containing the BH3 domain of Bad (NLWAAQRYGRELRRMSDEF VDSFKK) or Noxa (VPADLKDECAQLRRIGDKVNLRQKL) also were synthesized and purified to 95% purity (Mimotopes, Clayton, Victoria, Australia).

Generation of recombinant HCV. The pFL-J6/JFH-1 plasmid encoding the entire viral genome of a chimeric strain of HCV genotype 2a, J6/JFH-1 (37), was kindly provided by C. M. Rice, Center for the Study of Hepatitis C, The Rockefeller University. To generate mutant virus possessing a core protein mutation, a nucleotide substitution was introduced into pFL-J6/JFH-1 by site-directed mutagenesis using a QuikChange site-directed mutagenesis kit (Stratagene, La Jolla, CA). All PCR-amplified DNA fragments were verified extensively using an ABI PRISM 3100-Avant Genetic Analyzer (Applied Biosystems, Foster City, CA). Each of the plasmids was linearized by XbaI digestion and in vitro transcribed by using T7 RiboMAX (Promega) to generate the full-length viral genomic RNA. The in vitro-transcribed RNA (10 μg) was transfected into Huh7.5 cells by means of electroporation (975 μF, 270 V) using a Gene Pulser (Bio-Rad). The cells then were cultured in complete medium, and the supernatant was propagated as a virus stock. Culture supernatants of uninfected cells served as a control (mock preparation). Virus infectivity was measured by indirect immunofluorescence as previously described (17) and expressed as cell-infecting units (CIU) per milliliter.

Proliferation, caspase-3, and DNA fragmentation assays. Huh7.5 cells were seeded in 96-well plates at a density of 1.0×10^4 cells per well and cultured overnight. The cells then were infected with recombinant HCV at a multiplicity of infection of 0.1 CIU/cell or with a mock preparation. At different time points postinfection (p.i.), cell viabilities were determined by WST-1 proliferation assays (Roche, Mannheim, Germany) as described previously (17, 48).

Caspase-3 and DNA fragmentation assays also were performed on the infected cells as previously described (17).

HCV RNA quantitation. To measure intracellular HCV RNA replication levels, total RNA was extracted from the cells using an RNeasy Mini kit (Qiagen, Valencia, CA) according to the manufacturer's instructions. One microgram of total RNA was reverse transcribed using a QuantiTect reverse transcription kit (Qiagen) with random primers and was subjected to quantitative real-time PCR analysis using SYBR premix Ex *Taq* (Takara Bio, Kyoto, Japan) in a MicroAmp 96-well reaction plate and an ABI PRISM 7000 (Applied Biosystems, Foster, CA). The primers used to amplify an NS5A region of the HCV genome were 5′-AGACGTATTGAGGTCCATGC-3′ (sense) and 5′-CCGCAGCGACGGTG CTGATAG-3′ (antisense). As an internal control, human glyceraldehyde-3-phosphate dehydrogenase expression levels were measured using primers 5′-G CCATCAATGACCCCTTCATT-3′ (sense) and 5′-TCTCGCTCCTGGAAGA TGG-3′ (antisense).

Statistical analysis. Either the two-tailed Student's *t* test or one-way analysis of variance (using SPSS version 16.0) was applied to evaluate the statistical significance of differences measured from the data sets. $P < 0.05$ was considered statistically significant.

RESULTS

A BH3-like domain is present in the core protein. The family of Bcl-2 proteins constitutes one of the biologically important gene products in the regulation of apoptosis (see recent reviews in references 1, 16, 67, and 75). The Bcl-2 proteins may be classified broadly into three classes: prosurvival members containing multiple Bcl-2 homology domains, proapoptotic members containing multiple Bcl-2 homology domains, and proapoptotic members containing the BH3 domain only. The examination of the amino acid sequence of the core protein revealed that there is a BH3-like domain near the C terminus. An alignment of this domain with BH3 domains of the Bcl-2 family of proteins is shown in Fig. 1A. The BH3-like domain of the core protein contains L (residue 119) and D (residue 124)

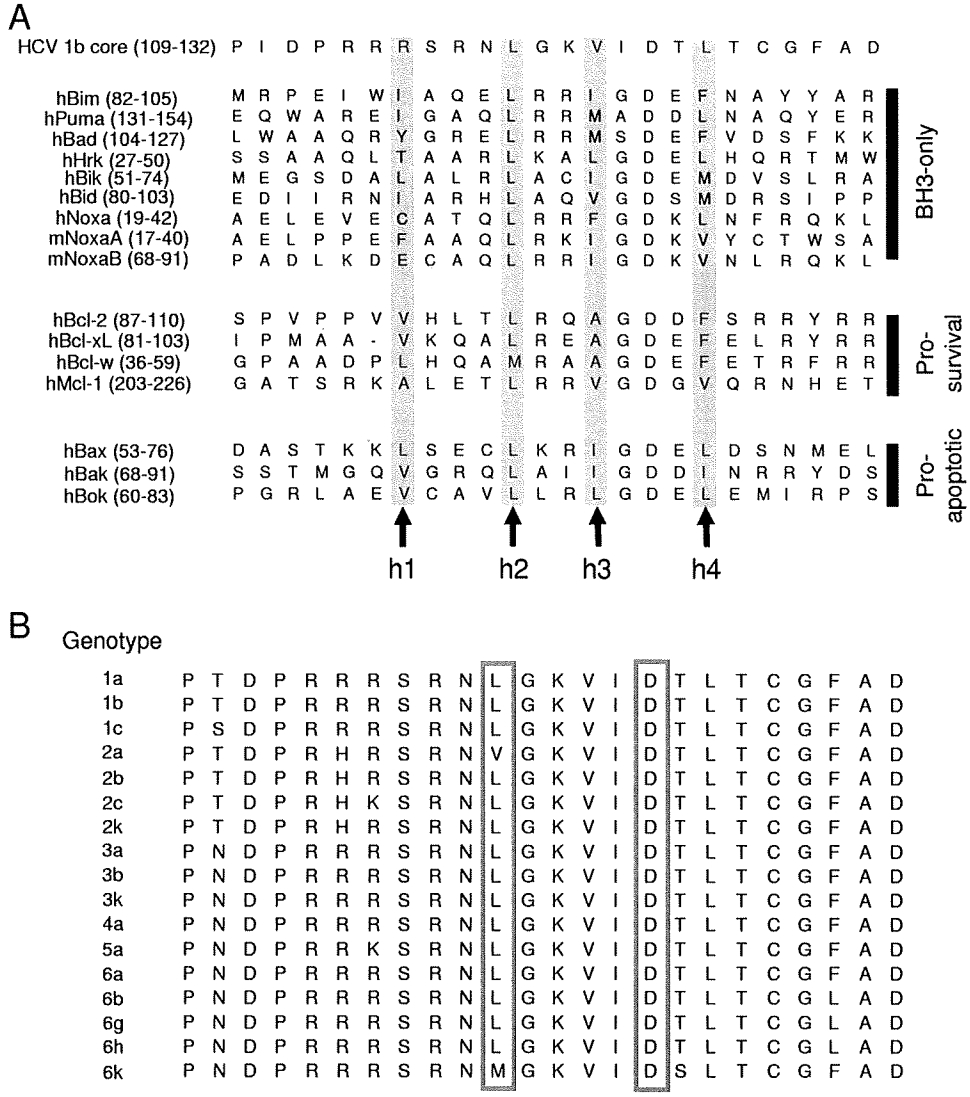

FIG. 1. Identification of a BH3-like domain in the core protein. (A) Alignment of the BH3 domain of the genotype 1b core protein with the BH3 domains of members of the Bcl-2 family. Numbers in parentheses represent the positions of amino acid residues of the respective proteins. The four hydrophobic amino acids that make critical contacts with residues in the BH3 recognition grooves present on the surfaces of the prosurvival Bcl-2 family proteins are indicated as h1 to h4. (B) Alignment of the core protein (residues 109 to 132) of different genotypes. The consensus sequences for these genotypes were obtained from http://hcv.lanl.gov/content/hcv-index. The highly conserved L and D residues, at positions 119 and 124 of the genotype 1b core protein, respectively, in BH3 domains are boxed.

separated by four residues, as in other known BH3 domains. This domain is highly conserved among the major HCV genotypes, with the exception of genotypes 2a and 6k, which have V and M residues at position 119, respectively (Fig. 1B).

The BH3 domain of the core protein is essential for the induction of apoptosis and its interaction with human Mcl-1. The overexpression of the core protein (with a flag epitope at the N terminus) in Huh7 cells, via the transient transfection of a cDNA expression plasmid containing the genotype 1b core protein gene, induced significant levels of apoptosis as determined by the activation of caspase-3, which is a hallmark of apoptosis (Fig. 2A). The deletion of the BH3 domain in the core protein (designated coreΔ115-128aa) abolished its proapoptotic property, indicating that this domain is essential for the induction of apoptosis. Consistently, the cleavage of endogenous PARP, a substrate of activated caspase-3, was clearly observed in Huh7 cells expressing the wild-type core protein but not in those expressing coreΔ115-128aa (Fig. 2B).

To understand how the core protein modulates the function of the Bcl-2 family of proteins, coimmunoprecipitation experiments were performed to determine if the core protein can interact with representative prosurvival members of the Bcl-2 family. As shown in the top panel of Fig. 3A, Mcl-1 was specifically coimmunoprecipitated by the core protein (lane 8) but not by an irrelevant protein, glutathione *S*-transferase (GST) (lane 7). The BH3 domain of the core protein is essential for its interaction with Mcl-1, as coreΔ115-128aa failed to coimmunoprecipitate Mcl-1 (lane 9). These results indicate that the core protein induces apoptosis by interfering directly with the prosurvival function of Mcl-1. In contrast, no significant inter-

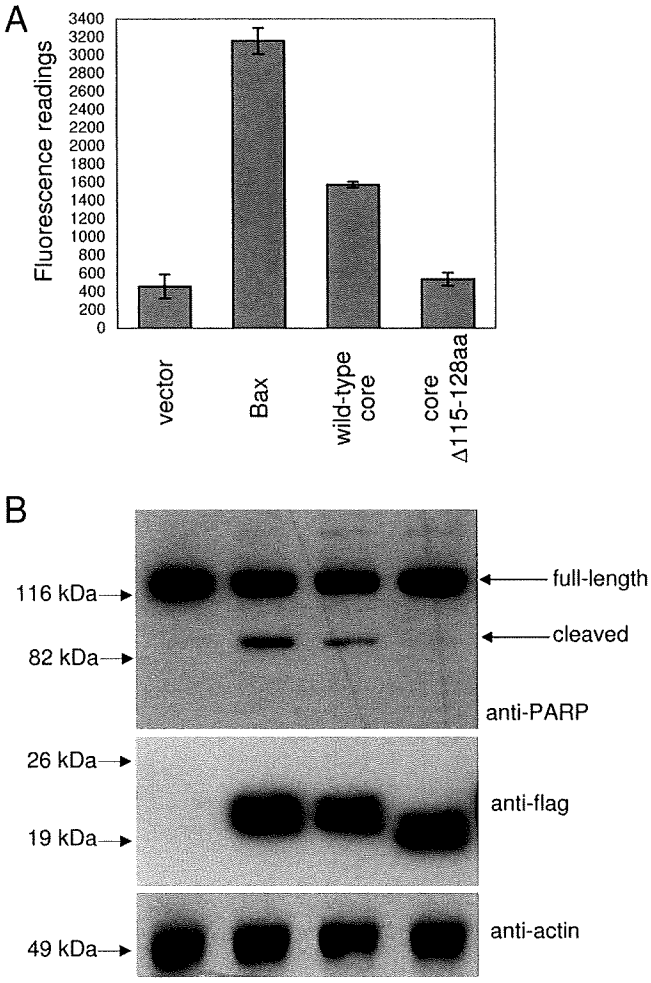

FIG. 2. Induction of apoptosis by the overexpression of the core protein in Huh7 cells. (A) A CaspACE fluorometric assay system from Promega Corporation (Madison, WI) was used to measure the activation of caspase-3, which is a hallmark of apoptosis, in Huh7 cells that were transfected with vector only, a classical apoptosis inducer (Bax), the wild-type core protein, and a core protein mutant lacking the putative BH3 domain (coreΔ115-128aa). All experiments were performed in triplicate, and the average values with standard deviations are plotted. (B) Western blot analysis also was performed to determine the cleavage of endogenous PARP, which is a substrate of activated caspase-3, from 116 to 83 kDa (top). Similarly, the expression levels of the different proteins were determined using anti-flag antibody (middle). The amounts of total cell lysates loaded were verified by measuring the levels of endogenous actin (bottom).

action was observed between the core protein and two other prosurvival proteins, Bcl-X_L and Bcl-w (lanes 1 to 6).

The interaction between the core protein and endogenous Mcl-1 was determined by overexpressing the core protein in Huh7 cells. As shown in Fig. 3B, the core protein was coimmunoprecipitated with endogenous Mcl-1 (lane 3). On the other hand, the core protein was not coimmunoprecipitated when an irrelevant antibody (anti-HA) (lane 4) was used for IP. Consistently with the results in Fig. 3A, only a small amount of coreΔ115-128aa was coimmunoprecipitated with endogenous Mcl-1 (lane 5). To estimate the degree of reduction in the binding of coreΔ115-128aa to endogenous Mcl-1, an imaging densitometer was used to quantify the intensities of specific bands on the autoradiographs obtained in three independent coimmunoprecipitation experiments (see Fig. S1 in the supplemental material). The ratios of signals for the expression of flag-tagged core protein, endogenous Mcl-1, and actin (internal control) all are close to 1 (0.94 to 1.14), indicating that the expression levels of these proteins in the two sets of cells (either transfected with cDNA construct for expressing flag-core or flag-coreΔ115-128aa) were similar. From the three independent experiments, the average amount of coreΔ115-128aa coimmunoprecipitated specifically by the Mcl-1 antibody is 14.2% (± 10.7%) of the amount of wild-type core protein coimmunoprecipitated. This implies that the deletion of the BH3 domain does not completely abolish the interaction between the core protein and endogenous Mcl-1 but reduces the interaction greatly.

Overexpression of Mcl-1 or Bcl-X_L prevents core protein-induced apoptosis. To examine the protective effects of the prosurvival Bcl-2 proteins in Huh7 cells, transfections were performed with plasmids expressing myc-tagged Bcl-2, Bcl-X_L, Bcl-w, or Mcl-1 (Fig. 4A and B). Consistent with studies of other cell lines (12, 66), the transient high-level expression of Bcl-2 also caused apoptosis in Huh7 cells (lane 1). Interestingly, the overexpression of Bcl-w also induced a significant level of apoptosis in Huh7 cells (lane 3), and this phenomenon has not been reported previously. Cells overexpressing Bcl-X_L, but not Mcl-1, also had a slightly higher level of apoptosis than that of the vector control cells (lanes 2 and 4).

Huh7 cells were cotransfected with plasmids for expressing myc-Mcl-1 and flag-core or myc-Bcl-X_L and flag-core. As shown in Fig. 4C and D, the level of apoptosis was significantly reduced in cells expressing both Mcl-1 and the core protein (lane 3) compared to those expressing the core protein only (lane 2). When the same experiment was repeated using Bcl-X_L, the level of apoptosis was reduced to a lesser extent (lane 5). However, this may be due to the low level of apoptosis induced by the overexpression of Bcl-X_L (lane 6). The level of the core protein expressed in the presence of Bcl-X_L also was decreased greatly, but the smaller amount of the core protein expressed still induced a high level of apoptosis (lane 5). However, when a broad caspase inhibitor (z-VAD-fmk) was used, the core protein level in cells coexpressing Bcl-X_L increased (see Fig. S2 in the supplemental material), indicating that the transfection efficiencies were similar in the different samples. To resolve this uncertainty, the experiment was repeated with a smaller amount of Bcl-X_L plasmid (0.5 μg). Under this condition, the overexpression of Bcl-X_L did not induce apoptosis (lane 8), and the level of apoptosis also was reduced in cells expressing both Bcl-X_L and the core protein (lane 7) compared to those expressing the core protein only (lane 2). Thus, the results show that the overexpression of either Mcl-1 or Bcl-X_L protects against core protein-induced apoptosis.

Bad enhances the ability of the core protein to release cytochrome *c* from isolated mitochondria. The ability of a core protein peptide, which contains residues 118 to 149 of the genotype 1b core protein, to release cytochrome *c* from the mitochondria was tested using 293T cells instead of Huh7 cells, as the method for the isolation of mitochondria from 293T cells is well established. The core protein induced apoptosis in 293T cells in the same manner as that in Huh7 cells (see Fig.

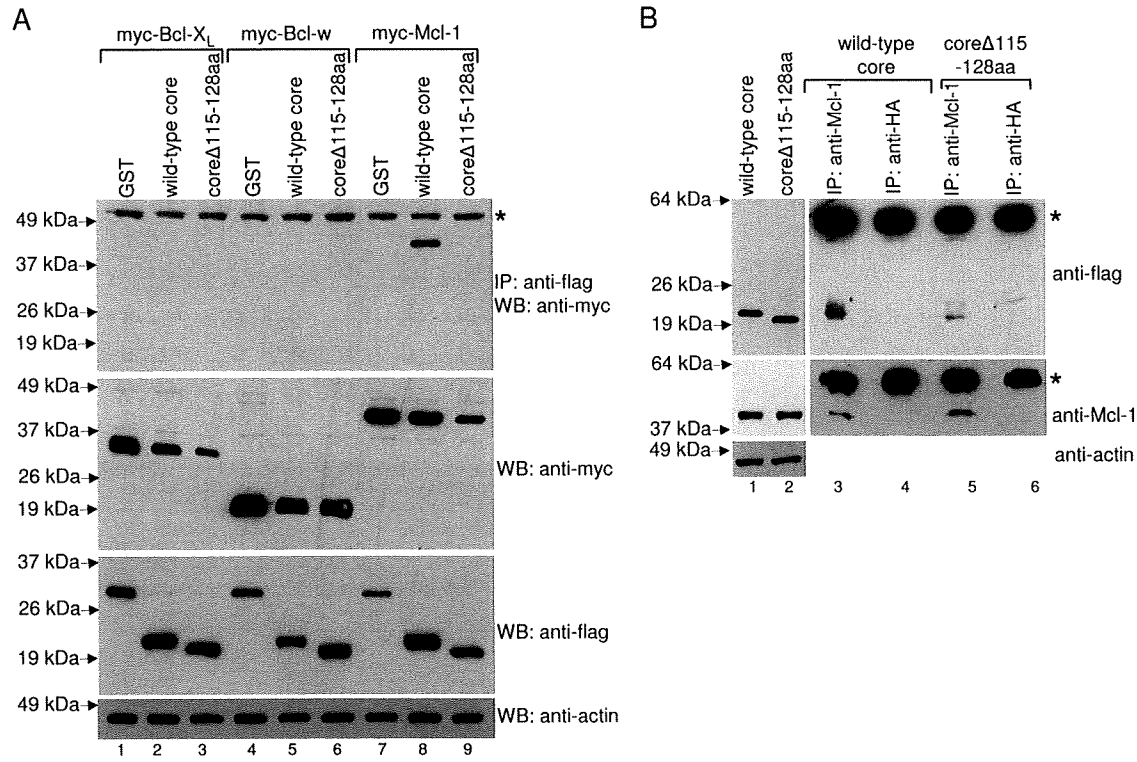

FIG. 3. Interaction of the core protein with prosurvival members of the Bcl-2 family determined by coimmunoprecipitation experiments. (A) Huh7 cells were transfected with cDNA constructs for expressing flag-GST (negative control), flag-core, or flag-coreΔ115-128aa, and myc-tagged prosurvival members of the Bcl-2 family (myc-Bcl-X_L [lanes 1 to 3], myc-Bcl-w [lanes 4 to 6], and myc-Mcl-1 [lanes 7 to 9]). The cells were harvested at ~16 h posttransfection, lysed, and subjected to IP with anti-flag monoclonal antibody conjugated to Sepharose beads. The amount of myc-tagged proteins that coimmunoprecipitated (IP) with the flag-tagged proteins was determined by Western blot analysis (WB) with an anti-myc rabbit polyclonal antibody (top). The amounts of myc-tagged and flag-tagged proteins in the lysates before IP were determined by subjecting aliquots of the lysates to Western blot analysis (middle). The protein marked with an asterisk represents the heavy chain of the antibody used for IP (top), and the amounts of total cell lysates loaded were verified by measuring the levels of endogenous actin (bottom). (B) Huh7 cells were transfected with cDNA constructs for expressing flag-core or flag-coreΔ115-128aa. IP then was performed using anti-Mcl-1 or anti-HA rabbit polyclonal antibodies and protein A agarose beads. The amounts of flag-tagged core protein in the lysates before IP (lanes 1 and 2) or coimmunoprecipitated (lanes 3 to 6) were determined by Western blot analysis with an anti-flag monoclonal antibody (top). Similarly, the amounts of endogenous Mcl-1 in these samples were detected using an anti-Mcl-1 monoclonal antibody (middle). The protein marked with an asterisk represents the heavy chain of the antibody used for IP (top), and the amounts of total cell lysates loaded were verified by measuring the levels of endogenous actin (bottom).

S3 in the supplemental material). As shown in Fig. 5A, both the Bad and core protein peptides were inefficient in inducing the release of cytochrome *c*, as only a small amount of cytochrome *c* was detected in the supernatant from the treated mitochondria when 200 μM of either peptide was used. However, when Bad and core protein peptides were used in combination, the release of cytochrome *c* was observed at the much lower concentration of 50 μM (consisting of 25 μM Bad peptide and 25 μM core protein peptide). Furthermore, the release of cytochrome *c* increased in a dose-dependent manner. The amount of cytochrome *c* left in the treated mitochondria (i.e., pellet) decreased correspondingly, while the amount of control protein, Hsp-60, was not affected.

The same experiment was repeated using the Noxa peptide (Fig. 5B). Consistently with a previous study (11), the Noxa peptide alone was inefficient in inducing the release of cytochrome *c*, but when it was combined with the Bad peptide, the release was significantly enhanced. The peptide(s) dosage required was similar to the amount required for the core protein and Bad, indicating that the complementation between the core protein and Bad is similar to the complementation between Noxa and Bad. In addition, complementation between the core protein and Bad also was observed when they were coexpressed in Huh7 cells (see Fig. S4 in the supplemental material).

The three hydrophobic residues in the BH3 domain of the core protein are important for apoptosis induction. Site-directed mutagenesis and structural studies of the interactions between the prosurvival Bcl-2 proteins and BH3 domains have revealed the mechanism by which BH3 domains are bound to the hydrophobic grooves present on the surfaces of the prosurvival Bcl-2 proteins (see reviews in references 50 and 69). In particular, the BH3 domain usually contains four hydrophobic residues (h1, h2, h3, and h4) (Fig. 1A) that make contacts critical for the stability of the complex. Interestingly, the core protein contains hydrophobic residues at the h2, h3, and h4 positions (Fig. 1A). An alanine substitution experiment was performed to determine if these residues are essential for the proapoptotic property of the core protein (Fig. 6A and B). The results showed that replacement of either L119, V122, or L126

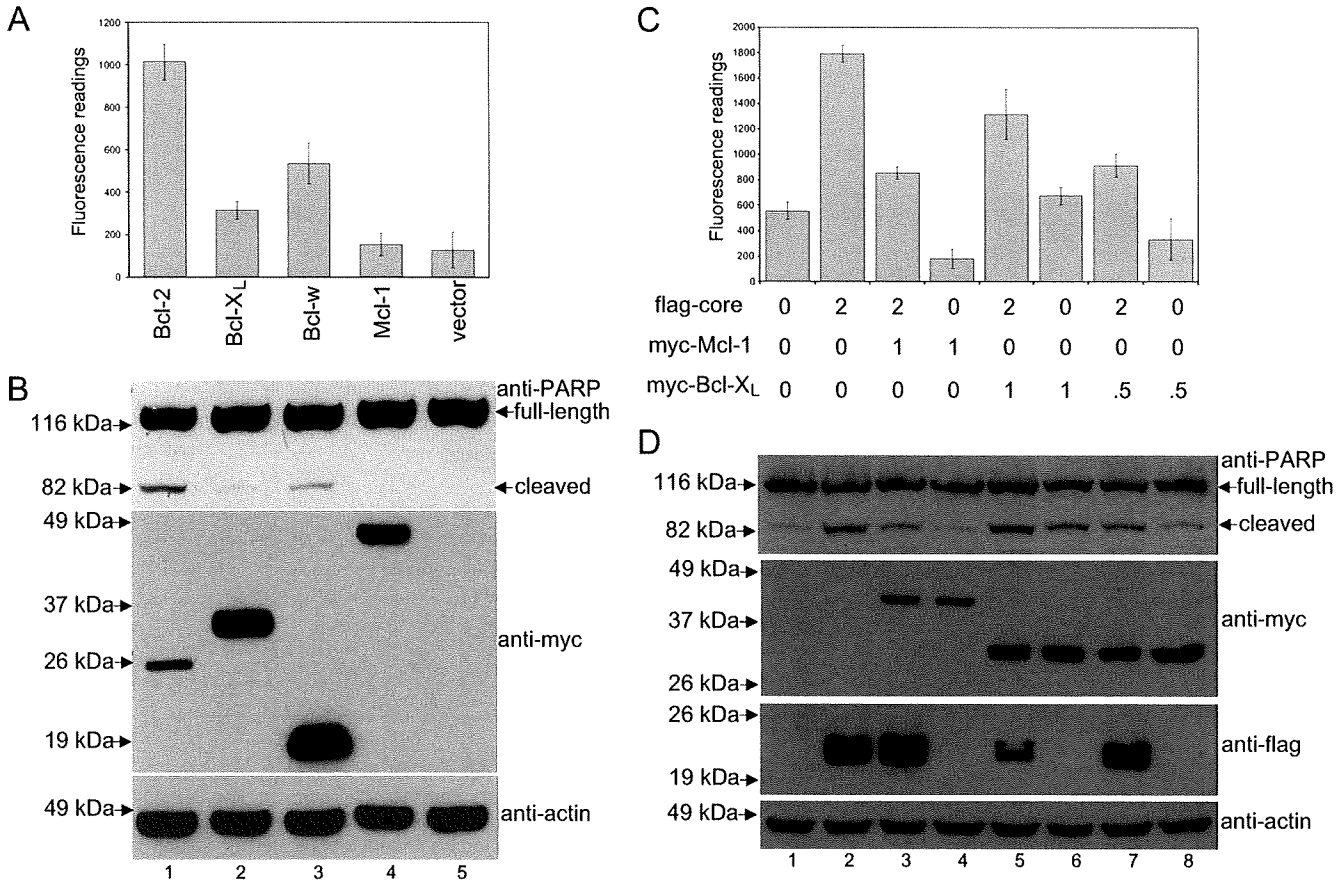

FIG. 4. Effects of Mcl-1 and Bcl-X_L overexpression on the proapoptotic property of the core protein. (A) A CaspACE fluorometric assay system from Promega Corporation (Madison, WI) was used to measure the activation of caspase-3 in Huh7 cells that were transfected with Bcl-2, Bcl-X_L, Bcl-w, Mcl-1, or vector only. All experiments were performed in triplicate, and the average values with standard deviations are plotted. (B) Western blot analysis also was performed to determine the cleavage of endogenous PARP (top) and expression levels of the myc-tagged prosurvival members of the Bcl-2 family (middle). The amounts of total cell lysates loaded were verified by measuring the levels of endogenous actin (bottom). (C) A CaspACE fluorometric assay system from Promega Corporation (Madison, WI) was used to measure the activation of caspase-3 in Huh7 cells that were singly transfected with vector, the wild-type core protein, Mcl-1, or Bcl-X_L, or that were cotransfected with wild-type core protein and Mcl-1 or Bcl-X_L. The amounts of flag-core and myc-Mcl-1 or myc-Bcl-X_L DNAs used in each of the transfections are indicated in micrograms. In each transfection, the total amount of DNA was normalized to 3 μg with the addition of empty vector if necessary. All experiments were performed in triplicate, and the average values with standard deviations are plotted. (D) Western blot analysis also was performed to determine the cleavage of endogenous PARP (top) and expression levels of myc-tagged Mcl-1 and Bcl-X_L and flag-tagged core protein (middle). The amounts of total cell lysates loaded were verified by measuring the levels of endogenous actin (bottom).

with A completely abolishes the proapoptotic property of the core protein. On the other hand, the replacement of the highly conserved D124 residue with A seems to increase the proapoptotic property of the core protein slightly. The levels of activated caspase-3 induced by the wild-type core protein and the D124A substitution mutant in six independent experiments were compared using the two-tailed Student's *t* test, and the difference was found to be statistically significant (Fig. 6C). This phenomenon has not been reported for other BH3-only proteins, but there are a few known functional BH3 domains that do not contain D at this position (54, 55).

Furthermore, coimmunoprecipitation experiments showed that the L119A, V122A, and L126A substitution mutants have reduced binding to Mcl-1 (Fig. 7A). Similar results were obtained in four independent experiments, and the percentages of binding compared to that of the wild-type core protein were estimated by using an imaging densitometer to measure the intensity of the core protein signals after coimmunoprecipitation. For each experiment, three different autoradiographs (with different exposure times) were used, and the average values are shown in Table S1 in the supplemental material. The average percentages in binding of Mcl-1 to the L119A, V122A, and L126A mutants are 33, 62, and 9% of the binding to the wild-type core protein, respectively. For all three mutants, the reduced interactions with Mcl-1 compared to those of the wild-type core protein are statistically significant (see Table S1 in the supplemental material). As the D124A substitution mutant induced a slightly higher level of apoptosis than the wild-type core protein (Fig. 6), a coimmunoprecipitation experiment also was performed to determine if this mutant can bind Mcl-1. Two different amounts of flag-tagged plasmids (0.5 and 1.0 μg) were used, and the results show that the D124A substitution mutant binds Mcl-1 to an extent similar to that of the wild-type core protein under both conditions (Fig. 7B).

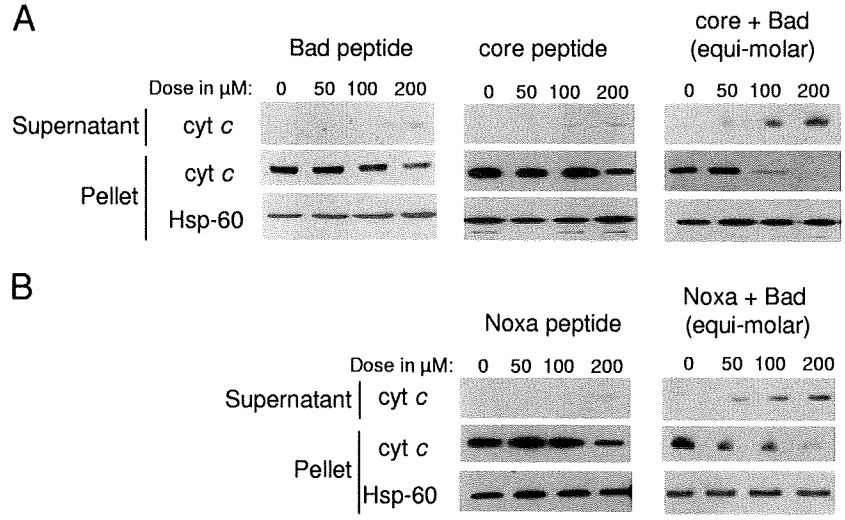

FIG. 5. Release of cytochrome *c* from isolated mitochondria by a combination of the core-BH3 and Bad-BH3 peptides or Noxa-BH3 and Bad-BH3 peptides. (A) Mitochondria isolated from 293T cells were incubated with either Bad peptide, core protein peptide, or a combination of the two peptides in equimolar concentrations. The total amount of peptide used in each experiment is indicated. Following centrifugation, the supernatants and pellets were subjected to Western blot analysis with anti-cytochrome *c* (cyt *c*) or anti-Hsp-60 antibodies. (B) The same experiment was repeated with Noxa peptide or a combination of Noxa and Bad peptides in equimolar concentrations.

While the V122 and L126 residues, at the h3 and h4 positions, respectively, of the core protein are highly conserved in different genotypes of HCV, the core proteins from genotype 2a strains typically have V instead of L at the h2 position (Fig. 1B). Replacing the L119 of the genotype 1b core protein with V reduced the proapoptotic property of the core protein dramatically (Fig. 8). Interestingly, in all known BH3-only proteins, this position is usually an L residue that is essential for the proapoptotic properties of these proteins (Fig. 1A). The reverse experiment was performed by determining if the core protein of a genotype 2a strain (JFH-1 strain) can induce apoptosis. The overexpression of the genotype 2a core protein induced much less apoptosis than the genotype 1b core protein (Fig. 8). However, replacing the V119 of the genotype 2a core protein with L resulted in a significant increase in apoptosis induction, such that the level was similar to that induced by the genotype 1b core protein (Fig. 8).

A single substitution from V to L at residue 119 in the core protein of the HCV J6/JFH-1 strain is associated with increased abilities to induce apoptosis. The pFL-J6/JFH-1 plasmid encoding the entire viral genome of a chimeric strain of HCV genotype 2a (J6/JFH-1) can be used to generate infectious HCV (37). In the J6/JFH-1 clone, the core protein contains V at residue 119, just like the JFH-1 clone. A mutant virus, J6/JFH-1(V119L), was generated successfully by replacing the V119 residue with L. Parental J6/JFH-1 and mutant J6/JFH-1(V119L) viruses then were used to infect naïve Huh7.5 cells, and cell viabilities were measured at different time points after infection (Fig. 9A). From day 2 p.i., cells infected by either virus have lower viabilities than mock-infected cells, indicating that the viruses have induced cytopathic effects (CPE). This is consistent with recent observations by us and other researchers (17, 41). Results from days 6 and 8 p.i. show that the J6/JFH-1(V119L) virus induced higher levels of CPE and, therefore, lower levels of cell viability compared to those of the parental J6/JFH-1 virus (Fig. 9A), which is in agreement with the overexpression studies shown in Fig. 8. The CPE is mediated primarily through apoptosis, as indicated by the activation of caspase-3 (Fig. 9B) and DNA fragmentation (Fig. 9C). The production of cell-free infectious virus particles by the J6/JFH-1(V119L) virus also was significantly higher than that produced by the parental J6/JFH-1 virus (Fig. 9D). On the other hand, there was no significant difference in the percentage of HCV-infected cells in the cultures (Fig. 9E) or HCV RNA replication in the cells between the two viruses (Fig. 9F). We next analyzed the possible interaction between endogenous Mcl-1 and the core proteins of either J6/JFH-1 or J6/JFH-1(V119L) in virus-infected cells. As shown in Fig. 9G, the core protein of J6/JFH-1(V119L) was coimmunoprecipitated with Mcl-1 (lane 6). On the other hand, the Mcl-1 interaction of the core protein of J6/JFH-1 was barely detected under the same experimental conditions (lane 4). These results collectively imply the possibility that the V119L mutation of the core protein promotes its interaction with Mcl-1 and is responsible for the increased ability of the virus to induce apoptosis, which favors a higher degree of infectious progeny virus release from the host cell at the late time points of infection compared to that of the parental J6/JFH-1 virus.

DISCUSSION

Besides playing important roles in maintaining homeostasis in healthy cells through the regulation of apoptosis, members of the Bcl-2 family also are involved in viral infections. Indeed, several viruses have been shown to encode homologs of prosurvival Bcl-2 proteins, and these viral proteins act to inhibit apoptosis in infected cells and prevent the premature death of these cells (see reviews in references 14, 26, 51, and 70). Other viral proteins, which can be proapoptotic, prosurvival, or both, do not share any sequence homology with members of the Bcl-2 family but also can modulate apoptosis in the host cells

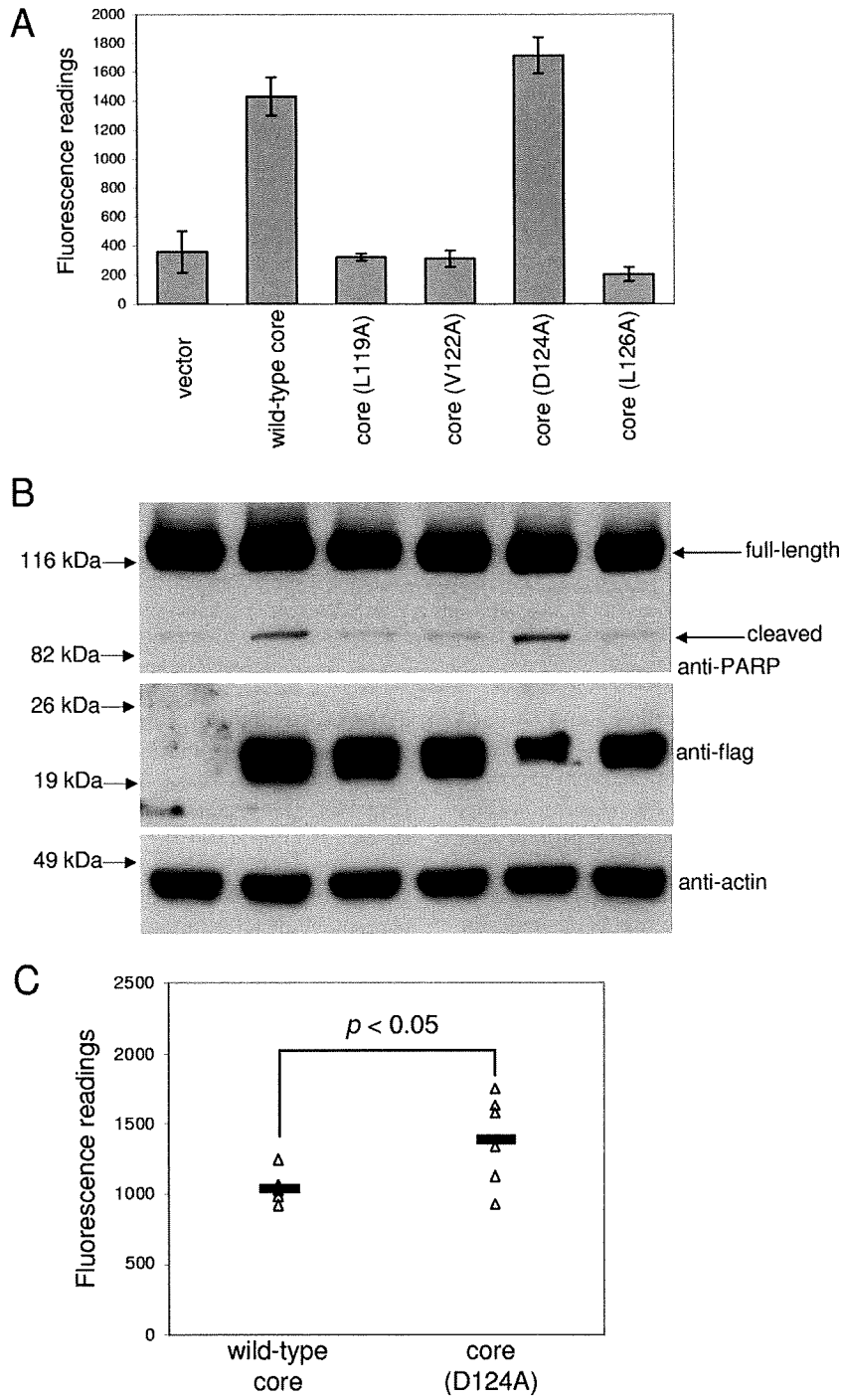

FIG. 6. Effects of alanine substitutions on the proapoptotic property of the core protein. (A) A CaspACE fluorometric assay system from Promega Corporation (Madison, WI) was used to measure the activation of caspase-3 in Huh7 cells that were transfected with vector only, wild-type core, or alanine substitution mutants. All experiments were performed in triplicate, and the average values with standard deviations are plotted. (B) Western blot analysis also was performed to determine the cleavage of endogenous PARP (top) and expression levels of the core proteins (middle). The amounts of total cell lysates loaded were verified by measuring the levels of endogenous actin (bottom). (C) The levels of activated caspase-3 induced by the wild-type core protein and the D124A mutant in six independent experiments were compared using the two-tailed Student's *t* test, and the difference was found to be statistically significant ($P < 0.05$). The values from each of the experiments are plotted as open triangles, and the average values are plotted as solid lines.

by interfering at different apoptotic checkpoints (see reviews in references 8, 23, 27, and 43).

Unlike the multi-BH domain members, the BH3-only members of the Bcl-2 family contain a single BH3 domain. Although all BH3-only proteins can bind to the hydrophobic grooves on the surfaces of the prosurvival members, recent quantitative measurements have revealed that the affinities of association between different pairs of BH3-only and prosur-

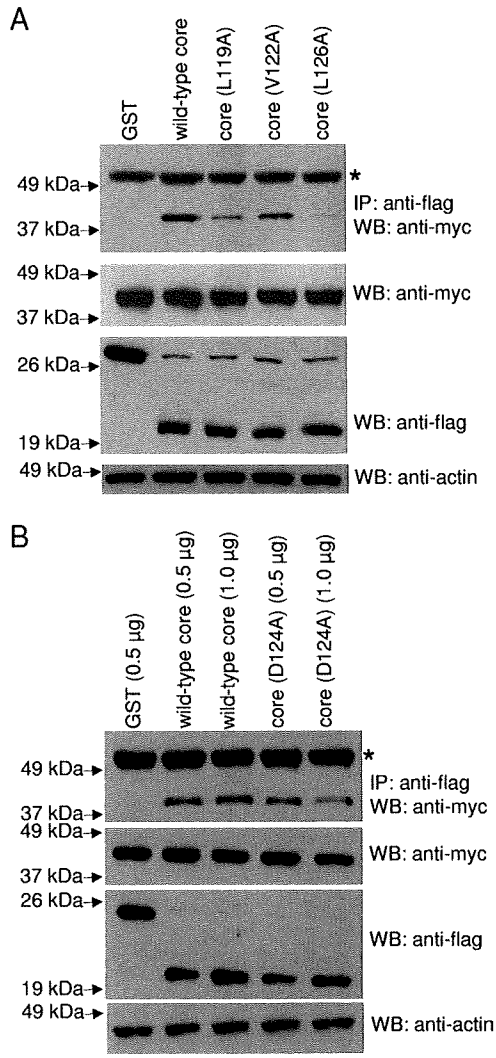

FIG. 7. Effects of alanine substitutions on the binding of the core protein to Mcl-1. (A) Huh7 cells were transfected with cDNA constructs (1.0 μg) for expressing flag-GST (negative control), flag-tagged wild-type core protein, or single-alanine-substitution mutants (L119A, V122A, and L126A). All cells were cotransfected with myc-tagged Mcl-1 (1.5 μg). (B) Huh7 cells were transfected with cDNA constructs for expressing flag-GST (negative control, 0.5 μg), flag-tagged wild-type core protein (0.5 or 1.0 μg), or single-alanine-substitution mutant D124A (0.5 or 1.0 μg). All cells were cotransfected with myc-tagged Mcl-1 (1.5 μg). Coimmunoprecipitation then was performed as described in the legend to Fig. 3A. The amount of myc-tagged proteins that coimmunoprecipitated (IP) with the flag-tagged proteins was determined by Western blot analysis (WB) with an anti-myc rabbit polyclonal antibody (top). The amounts of myc-tagged and flag-tagged proteins in the lysates before IP were determined by subjecting aliquots of the lysates to Western blot analysis (middle). The amounts of total cell lysates loaded were verified by measuring the levels of endogenous actin (bottom). The protein marked with an asterisk represents the heavy chain of the antibody used for IP (top). Similar results were obtained in four independent experiments, and a representative set of data is presented.

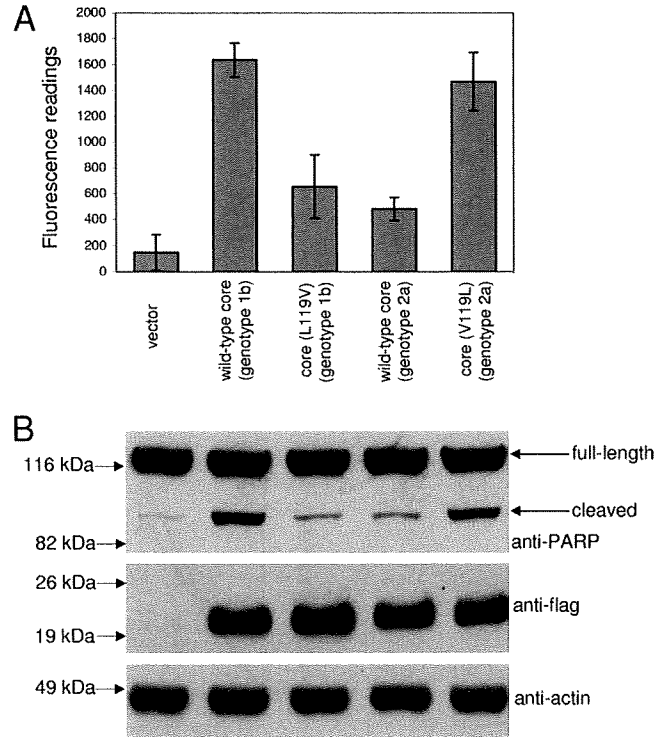

FIG. 8. Comparison of the proapoptotic properties of the core proteins of genotypes 1b and 2a. (A) A CaspACE fluorometric assay system from Promega Corporation (Madison, WI) was used to measure the activation of caspase-3 in Huh7 cells that were transfected with vector only, wild-type core of genotype 1b or 2a, or their substitution mutants. All experiments were performed in triplicate, and the average values with standard deviations are plotted. (B) Western blot analysis also was performed to determine the cleavage of endogenous PARP (top) and expression levels of the core proteins (middle). The amounts of total cell lysates loaded were verified by measuring the levels of endogenous actin (bottom).

vival members vary greatly (11, 32). For example, Bim and Puma bind all prosurvival members tested, while Noxa binds strongly only to Mcl-1 and A1. On the other hand, Bad binds much more strongly to Bcl-2, Bcl-X_L, and Bcl-w than Mcl-1.

Taken together with results from successive studies, it becomes clear that the BH3-only members can be classified into subclasses (see reviews in references 21, 24, 58, and 71). In this study, we demonstrate that the HCV core protein is a BH3-only viral homologue of the Bcl-2 family, and its BH3 domain is essential for the induction of apoptosis (Fig. 1 and 2). In coimmunoprecipitation experiments, the core protein interacted specifically with the prosurvival Mcl-1 protein but not with prosurvival proteins Bcl-X_L and Bcl-w (Fig. 3), suggesting that its property is most similar to that of Noxa (11). Consistently, the overexpression of Mcl-1 protects against core protein-induced apoptosis (Fig. 4). However, the overexpression of Bcl-X_L also protects against core protein-induced apoptosis (Fig. 4). This may be due to the ability of a high level of Bcl-X_L to prevent the complementation between the core protein and endogenous Bad protein, which binds strongly to Bcl-X_L (11), as we have observed that a combination of the core protein and Bad peptide mimetics caused efficient cytochrome *c* release from the mitochondria (Fig. 5). The complementation between Bad and the core protein is similar to that observed between Bad and Noxa, which act in combination to neutralize the two classes of prosurvival proteins, one comprised of Bcl-2, Bcl-X_L, and Bcl-w and the other of Mcl-1 and A1 (11). In overexpres-

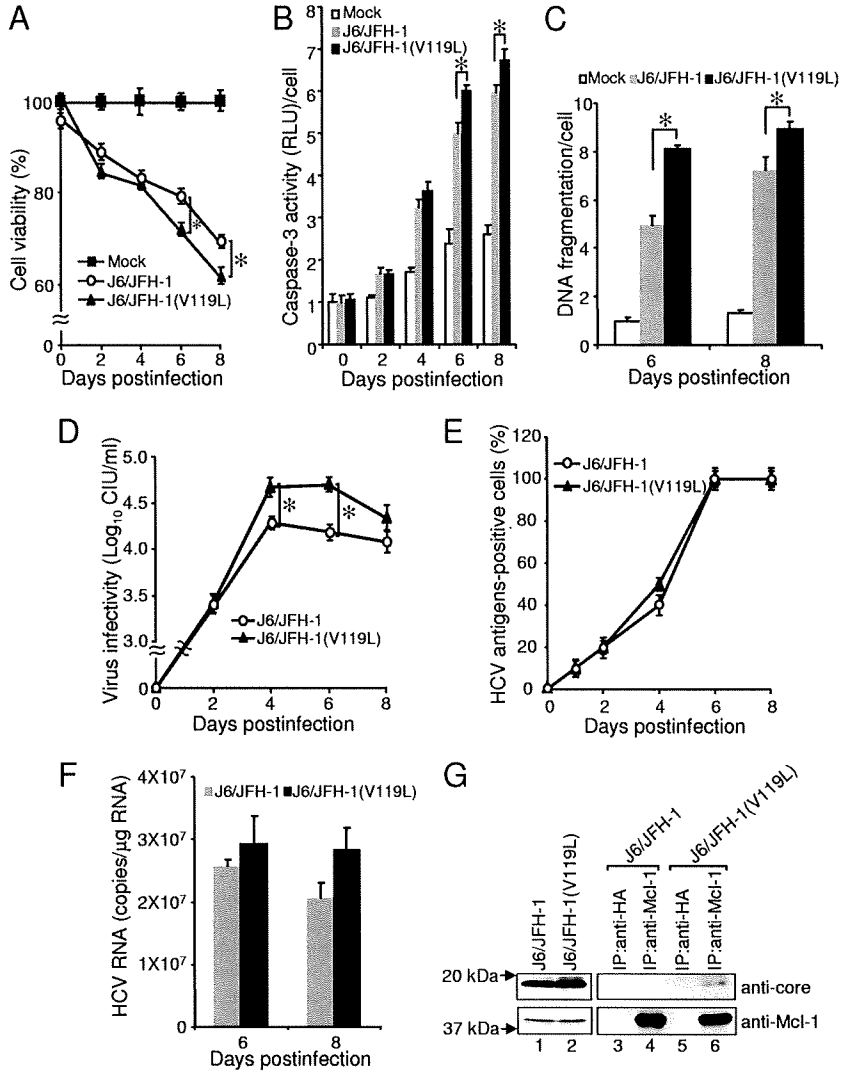

FIG. 9. Comparison of parental J6/JFH-1 and mutant J6/JFH-1(V119L) recombinant viruses. Huh7.5 cells were infected with recombinant HCV at a multiplicity of infection of 0.1 CIU/cell or with a mock preparation, and various assays were performed at different days after infection. (A) Cell viabilities were determined. (B) Caspase-3 activity per cell was determined. (C) The amount of DNA fragmentation per cell was determined. (D) The production of cell-free infectious virus particles was determined. (E) Virus spread in the culture was quantitated. (F) HCV RNA replication was determined by quantitative real-time PCR analysis. (G) Interaction of the core protein with Mcl-1 was determined by coimmunoprecipitation experiments at 3 days p.i. IP was performed using anti-Mcl-1 or anti-HA rabbit polyclonal antibodies and protein A agarose beads. The amounts of the core protein in the lysates before (lanes 1 and 2) and after IP (lanes 3 to 6) were determined by Western blot analysis with an anti-core monoclonal antibody (top). Similarly, the amounts of endogenous Mcl-1 in the samples were determined using an anti-Mcl-1 monoclonal antibody (bottom). Statistical analysis was performed using the one-way analysis of variance to determine if the differences between parental and mutant viruses were statistically significant, and those with P values of <0.05 (marked by asterisks) are considered statistically significant. Data were obtained from three independent experiments, each with triplicate cultures.

sion studies, the core protein and Noxa also induced comparable levels of apoptosis (see Fig. S3 and S5 in the supplemental material). Taken together, these findings suggest that core can mimic Noxa and interfere directly with the prosurvival function of Mcl-1.

A comparison of the BH3 domain of the core protein to the corresponding domains of other BH3-containing proteins (Fig. 1A) revealed that it contains three out of the four hydrophobic residues that can be accommodated within the hydrophobic pockets of previously described BH3 binding grooves (see reviews in references 50 and 69). Alanine substitution experiments revealed that all three hydrophobic residues in the BH3 domain of the core protein are essential for apoptosis induction (Fig. 6). In coimmunoprecipitation experiments, these alanine substitution mutants also bound Mcl-1 to a lesser extent than the wild-type core protein (Fig. 7A). Since these alanine substitution mutants still can bind Mcl-1, albeit at a lower level than that of the wild-type core protein, it appears that the interactions between these mutants and Mcl-1 are not sufficient to induce apoptosis. In several mutagenesis studies, the interaction between Bcl-2 family members and apoptosis regulation have been observed to be discordant. For example, two mutants of the BH3-only protein Bik, Bik-(43-94) and Bik-(43-120), heterodimerized with prosurvival Bcl-2 and Bcl-X_L but

were unable to induce efficient cell death (19). A Bad mutant containing an alteration of a critical residue within its BH3 domain, E113 to K, also was found to have significantly reduced apoptotic activity compared to that of wild-type Bad, despite binding to Bcl-2 and/or Bcl-X_L to the same extent as wild-type Bad (35). Therefore, the induction of apoptosis by the core protein may be controlled by a critical threshold affinity of binding between the core protein and Mcl-1, or there are contributions from a yet-to-be characterized pathway(s). Two of these residues (V122 and L126) are conserved in the major genotypes of HCV, but residue 119 is a V in genotype 2a (Fig. 1B). When L119 of the genotype 1b core protein was replaced with V, its ability to induce apoptosis was greatly reduced (Fig. 8). Conversely, when V119 of the genotype 2a core protein was replaced with L, its ability to induce apoptosis was greatly enhanced. Thus, the results suggest that the genotype 1b core protein induces apoptosis efficiently via a BH3 domain, while genotype 2a core protein is comparatively less efficient. Another highly conserved residue in the BH3 domain of the core protein is D124. However, the replacement of D124 with A did not reduce the proapoptotic function of the core protein (Fig. 6). Thus far, there are only a few known functional BH3 domains that do not contain D at this position (61, 62). Unlike most BH3-only proteins, the core protein has a charged residue (R115) in the h1 position (Fig. 1A). Interestingly, the second BH3 domain of mouse Noxa (mNoxaB) also has a charged residue (E74) in this position. Indeed, the nuclear magnetic resonance structure of the complex between mouse Mcl-1 and a peptide mimetic of mNoxaB shows that E74 is tolerated at the h1 position because its charged carboxyl group is coordinated by another charged residue, K215, in mouse Mcl-1 (15). However, R115 of the core protein is basic instead of acidic, and how this residue can be accommodated in the hydrophobic groove of Mcl-1 is unclear. Interestingly, replacing the residue at the h1 position (I58) of a novel BimBH3 variant, Bim_s2A, with A also has little effect on its interaction with Mcl-1 (34). Thus, it appears that the residue in the h1 position is not always involved in the interaction between BH3-only proteins and Mcl-1, but further biophysical and biochemical studies are required to delineate the precise structure-function relationship for the interaction between core and Mcl-1.

To determine if the results from overexpression studies are relevant to the modulation of apoptosis in host cells during HCV infection, the J6/JFH-1-based (genotype 2a) system was used to generate HCV carrying a substitution at residue 119 of the core protein. While the parental wild-type and mutant viruses replicated efficiently in Huh7.5 cells, the J6/JFH-1(V119L) virus (which expresses the core protein with L at the h2 position of the BH3 domain) caused a significantly higher level of apoptosis in the infected cells than the parental J6/JFH-1 virus (which expresses the core protein with V at the h2 position of the BH3 domain) (Fig. 9). This is in good agreement with the overexpression studies and indicates that the BH3 domain of the core protein contributes to the induction of apoptosis in HCV-infected cells. Thus, it appears that core protein-mediated apoptosis during infection by HCV of genotype 2a is less efficient than that of the other genotypes having L at residue 119 of the core protein (Fig. 1B). Coimmunoprecipitation experiments revealed that the core protein of J6/JFH-1(V119L), but not that of J6/JFH-1, interacted with Mcl-l in virus-infected cells (Fig. 9). This result is consistent with the overexpression studies and suggests the possibility that the core protein induces apoptosis, at least partly, through the interaction with Mcl-1 in HCV-infected cells. Interestingly, more progeny virus is released from cells infected with the J6/JFH-1(V119L) virus than by those infected with the parental J6/JFH-1, while there is no difference in the efficiency of infection or amount of HCV replication inside the cells (Fig. 9).

However, it also is apparent that the parental J6/JFH-1 virus still caused a high level of apoptosis in the infected cells, and for the early time points there was no significant difference in the levels of apoptosis induced by the parental J6/JFH-1 virus and the J6/JFH-1(V119L) mutant virus (Fig. 9). This implies that there are other viral factors that contribute to the induction of apoptosis during HCV infection. For example, several nonstructural HCV proteins, like NS3, NS4A, NS5A, and NS5B, can induce apoptosis when they are overexpressed in certain types of cells (see recent reviews in references 20 and 28). In addition, other domains in the core protein have been shown to bind host proteins and may contribute to apoptosis regulation by interfering with different cellular pathways (see reviews in references 33, 42, and 52). For example, the N-terminal domain (aa 1 to 75) of the core protein interacts with Hsp60, leading to the production of reactive oxygen species and enhancement of tumor necrosis factor alpha-mediated apoptosis (30), while a C-terminal domain (aa 153 to 192) facilitates Fas oligomerization and is required for apoptosis induction in Jurkat cells (46). However, the relative contribution of these various factors to apoptosis induction during HCV infection remains to be determined.

We further examined the importance of residue 119 of the core protein in HCV replication. In multiple independent transfection experiments, we observed that the J6/JFH-1 mutant possessing A at position 119 [J6/JFH-1(V119A)] barely replicated in the cells and did not produce any infectious virus particles in the culture supernatants (data not shown). This result suggests the possibility that this single point mutation impairs the interaction of the core protein with other viral and/or cellular protein(s) that is required for HCV RNA replication and infectious virion production. Similarly, the J6/JFH-1 mutants each possessing A at positions 122 [J6/JFH-1(V122A)], 124 [J6/JFH-1(D124A)], or 126 [J6/JFH-1(L126A)] barely replicated in the cells and did not produce any infectious virion in the culture supernatants (data not shown), with the results suggesting an important role(s) for these residues as well as for position 119. In this connection, the essential role for the HCV core protein in infectious virion production recently has been confirmed, and numerous residues required for this role have been identified (47).

By using the JFH-1 infectious clone, recent studies have revealed that the association of the core protein with the lipid droplet (LD) is critical for the production of infectious virus particles (6, 45). Boulant and coworkers reported that there are two amphipathic α-helices in the so-called D2 domain of the core protein (~118 to 179 aa) (5, 7), and the hydrophobic residues within this domain are critical for the efficient attachment of the core protein to LD (5). Our results showed that residues L119, V122, and L126 of the core protein are essential